Supraglacial hydrology and dynamic changes through the 2021-2022 surge of Nàlùdäy (Lowell Glacier), Yukon.

Jaime Dubé

A thesis submitted to the University of Ottawa in partial fulfillment of the requirements for the Master of Science degree in Geography

Supervisor
Dr. Luke Copland

Thesis Committee
Dr. Gabrielle Kleber
Dr. Anders Knudby

Department of Geography, Environment and Geomatics
Faculty of Arts
University of Ottawa

Abstract

Nàłùdäy's (Lowell Glacier) most recent surge had a two-phase initiation, with the first phase beginning in spring 2021 at the terminus following a calving event that took place the previous winter. The second acceleration phase began in fall 2021 with surge velocities peaking in spring 2022, before returning to quiescence by late fall 2022. The total length of streams on the glacier surface pre- to post surge dropped by over 50%, with the resulting supraglacial system transporting water less efficiently. The location of the second acceleration coincides with a clustering of moulins which provided water inputs to a subglacial overdeepening. This surge highlights the connection between supraglacial hydrology and surge dynamics, where surge initiation is driven by water input location and subglacial topography, and supraglacial hydrology is impacted by surface changes driven by ice deformation and basal sliding during the surge.

Acknowledgements

Firstly, I would like to acknowledge that the research presented in this thesis takes place on the traditional territory of the Champagne and Aishihik First Nations. I would like to thank the community for allowing me to do this research, and present and discuss it with members at various stages throughout the last two years. I also want to acknowledge that this research focuses on a western science view of glacier changes in the St. Elias Mountains. There is a lot of traditional knowledge held in the community that is not discussed in this thesis, that holds valuable information about the movement and history of glaciers in the region.

This thesis would not have been possible without the support of my supervisor, Dr. Luke Copland. Thank you for all your help throughout the last two years, for trusting me with many opportunities, and for teaching me everything I know about glaciers. I would also like to thank Dr. Gabrielle Kleber and Dr. Anders Knudby for being on my committee. I would like to acknowledge that this research would not have been possible without the support of numerous organisations, including the University of Ottawa Department of Geography, Environment and Geomatics, the Natural Sciences and Engineering Research Council of Canada (NSERC) Discovery Grant and Northern Supplement, the Polar Continental Shelf Program (PCSP), the Royal Canadian Geographical Society (RCGS), ArcticNet and the Kluane Lake Research Station.

Thank you to the members of the Laboratory for Cryospheric Research for your support, advice and friendships over the last few years. I'm extremely grateful for all the time spent in the field and on glaciers the past two years, from multiple summers in Kluane, to a month on Axel Heiberg, I've learned more than I could have possibly imagined from these experiences. I am also thankful for all the training opportunities I've had in the past 2 years, including courses at the University of Ottawa, the University Centre in Svalbard (UNIS), and with the European Space Agency.

Lastly, I would like to thank my family and friends, both in Ottawa and back home, for your support, and Aspen, for always reminding me to take breaks and go outside.

Preface

This thesis is written in a hybrid format, with Chapter 1 introducing the subject matter, providing a literature review, and describing the overall objectives of the MSc project. Chapter 2 is a research article pertaining to the 2021-2022 surge of Nàłùdäy. References for the entire thesis are provided in Chapter 3, and appendices in Chapter 4.

Chapter 2 will undergo slight reformatting to meet journal requirements, and co-author review, before being submitted to the Journal of Glaciology. The proposed title and list of authors for the article is:

Dubé, J., Copland, C., Dow, C., Main, B., Medrzycka, D. & Wray, P. Linking supraglacial hydrology and surge dynamics during the 2021-2022 surge of Nàłùdäy (Lowell Glacier), Yukon, Canada.

I am the primary author of both Chapters 1 & 2, and undertook the lead in all writing, data collection, data processing and interpretation. My thesis supervisor, Dr. Luke Copland, provided input and guidance throughout the entire planning, data processing and writing process. For Chapter 2, Dr. Luke Copland and Dr. Christine Dow (University of Waterloo) also contributed to field planning and logistics, and provided in-situ data and air photo surveys for Nàłùdäy. Dr. Brittany Main and Dr. Dorota Medrzycka collected field data prior to when I began my program in summer 2023, and provided training in fieldwork and processing procedures for velocity image processing (Main) and Structure from Motion reconstructions (Medrzycka). Peter Wray provided the bed topography based on AirIPR (airborne ice penetrating radar) measurements of Nàłùdäy.

Table of Contents

List of Figures

List of Tables

Abbreviations

a.s.l.	Above Sea Level
AutoRIFT	Autonomous Repeat Image Feature Tracking
DEM	Digital Elevation Model
EDW	Elevation-dependent Warming
ESA	European Space Agency
ITS_LIVE	Inter-Mission Time Series of Land Ice Velocity and Elevation
IW	Interferometric Wide Swath
NASA	National Aeronautics and Space Administration
NDWI	Normalised Difference Water Index
$NDWI_{ice}$	Normalised Difference Water Index for ice
PDDs	Positive Degree Days
RGI	Randolph Glacier Inventory
SAR	Synthetic Aperture Radar
SfM	Structure from Motion
SLE	Sea Level Equivalent

Chapter 1: Background and research objectives

1.1. Glacier hydrology and its influence on dynamics

The three main hydrological systems present on glaciers are supraglacial (surface), englacial (interior) and subglacial (basal). The makeup of these systems and their connectivity play a crucial role in determining glacier dynamics. Hydrological connections between the surface and basal systems are controlled in part by a glacier's thermal regime, with the presence of cold ice (i.e., <0°C) limiting the ability for meltwater to reach the bed (Bingham et al., 2006), and the quantity and location of sinks. The hydrology of temperate and non-temperate glaciers may differ significantly depending on the thermal regime of the glacier (Irvine-Fynn et al., 2011), although their hydrological systems are still composed of the same main elements: i.e., supraglacial, englacial and subglacial. Understanding the individual components of each hydrological system, as well as their connectivity and link to dynamics, is therefore crucial for fully understanding the driving mechanisms behind glacier surges and other dynamic instabilities.

1.1.1. Supraglacial hydrology

Meltwater flows on the glacier surface through a system comprised of streams, channels and rivers, which can terminate prior to the end of the glacier in moulins, lakes or crevasses (Pitcher & Smith, 2019). Supraglacial hydrological systems have been studied in-situ (Knighton, 1981; Gleason et al., 2016; St Germain & Moorman, 2019), with remote sensing (Smith et al., 2015; King et al., 2016; Lu et al., 2020; Rawlins et al., 2023), and using models (Clason et al., 2012; Hill & Dow, 2021).

The term supraglacial channels encompasses both larger perennial rivers and transient (on seasonal to annual timescales) lower order streams present on the glacier surface (Pitcher & Smith, 2019). Supraglacial channels exhibit similar characteristics to streams in alluvial and other terrestrial environments (Karlstrom & Yang, 2016). They develop due to a combination of internal and external forcing, with internal forcing being a primary driver of supraglacial channel progression from channel incision, to channel wall ablation, to meandering of channels (Pitcher & Smith, 2019). Geometrical changes in the channel system are a response to surface topography and thermal erosion from flowing water (Karlstrom & Yang, 2016). The fluvial processes that cause

supraglacial stream development are thought to be transferable from glacier to glacier, although non-fluvial processes, including incoming solar radiation and surface topography, is dependent on the location of the glacier in question, as well as the orientation and location of the channels on the glacier surface (St Germain & Moorman, 2019).

Supraglacial lakes are generally found in areas with dips in bedrock topography, which create supraglacial depressions (Lampkin & VanderBerg, 2011). These lakes act as storage on the surface of the glacier for meltwater fed through supraglacial channels, until they occasionally drain suddenly to the subglacial hydrological system due to expanding hydrofracturing at the lake bed (Das et al., 2008; Chudley et al., 2019). Sudden drainages of supraglacial lakes supply large amounts of water to the glacier bed in short periods of time (a few hours), having impacts on glacier dynamics, with their importance likely underestimated in current literature (Chudley et al., 2019).

1.1.2. Englacial & subglacial hydrology

Englacial channels, including crevasses and moulins, act as conduits connecting the supraglacial hydrological system with the basal system and typically provide the main source of water to the glacier bed. Englacial conduits also exist in the body of a glacier, moving water horizontally across the glacier and connecting to vertically draining conduits (Fountain & Walder, 1998). Moulins are vertical or near-vertical channels which enable meltwater to flow to the basal hydrological system (Chu, 2014), typically forming where there are naturally occurring structural weak spots such as a crevasse, or crevasse field, where strain rates at the glacier surface are already high (Holmlund, 1988). Greater meltwater availability from increased air temperatures enables moulins to form earlier during the year, and at higher elevations on the glacier surface (Clason et al., 2012). There exists a possible feedback loop between increased meltwater production and drainage to the basal system, as an increase in meltwater inputs results in a larger tensile stress on the surface from longitudinal stretching, resulting in more fracture propagation on the glacier surface and thus more pathways for water to reach the glacier bed (Clason et al., 2012).

The subglacial hydrological system consists of a network of channels or cavities found at the base of a glacier. The hydrological system underneath the glacier develops due to a variety of variables, one of which being whether the ice sits directly on bedrock or unconsolidated sediment (soft-bedded). The soft-bedded subglacial hydrology theory describes a seasonally evolving anastomotic

braiding of subglacial channel system, where multiple channels split and connect at various locations, which is fully active in summer seasons (Hart et al., 2022). As meltwater inputs decrease, a portion of the water that was in subsidiary channels is stored within the subglacial system, with possible release or discharge occurring during positive degree days (i.e., days with air temperatures above 0°C). For glaciers sitting on hard bedrock, there are two main types of subglacial networks that may be present, channelized and distributed. A channelized system is made up of conduits either incised upwards into the ice ('R' or 'Röthlisberger' channel; Röthlisberger, 1972), downwards into bedrock ('N' or 'Nye' channel; Nye, 1965) or both, transporting water under the glacier (Benn & Evans, 1998; Fountain & Walder, 1998). Compared to fast water flow through a channelized system, the distributed subglacial system results in slow moving water flow through linked cavities at the bed of a glacier. This distributed or "linked-cavity" system is inefficient at transporting water from englacial channels to proglacial outputs (Fountain & Walder, 1998). Subglacial hydrological systems can also store water, delaying outputs, which often occurs seasonally (Chu et al., 2016).

1.1.3. Connections between glacier hydrology and ice dynamics

The dynamic movements of glaciers and ice sheets globally have been well linked to subglacial hydrology, which as described above is typically fed by supraglacial meltwater through englacial channels. Ice dynamics are usually quantified through variations in surface velocity, both horizontal and vertical. Short-term variations in glacier velocities can be observed at both seasonal and diurnal scales in response to changing meltwater inputs, typically driven by variations in local climate (Copland et al., 2003; Bingham et al., 2006; Smith et al., 2021). Increased meltwater inputs to the bed have been associated with short-term increases in surface velocity, likely caused by high basal pressure creating increased basal sliding (Bingham et al., 2006; Togaibekov et al., 2024). Diurnal cycling of water input at moulins and changes in glacier velocity have identified a cycling of the subglacial water storage system as well, where storage increases nightly as a delayed response to the pressurization of the subglacial hydrological system from daytime meltwater increase (Smith et al., 2021).

Many studies have outlined the seasonal evolution of subglacial drainage and its link to glacier dynamics (Willis, 1995; Fountain & Walder, 1998; Schoof, 2010; Chu, 2014). High water flow and pressure within a distributed subglacial system during early spring/summer generates high

glacier surface velocities. The consistent influx of large volumes of water during early melt season into the subglacial system facilitates the formation of an efficient channelized system, increasing effective overburden pressure at the bed (due to a decrease in basal water pressure) and reducing ice velocities (Schoof, 2010). As melt decreases during late summer/autumn efficient channels are closed by the inward creep of ice (Fountain & Walder, 1998), leaving a distributed subglacial drainage system. The distributed system remains over winter, until the spring influx of melt increases channelization in the subglacial system (Schoof, 2010) and the cycle repeats itself.

Velocity variations in response to meltwater influx can also be seen by regional responses within a glacier and over longer timescales. For example, velocity variations associated with meltwater inputs were highest closer to supraglacial sinks on Devon Ice Cap in the Canadian Arctic (Wyatt & Sharp, 2015). Similarly, sudden drainage of a supraglacial lake in Greenland resulted in changes in both horizontal and vertical velocities (Chudley et al., 2019). On a seasonal timescale, increased summer melt resulted in slower velocities recorded the following winter in Alaska, likely due to an increase in subglacial water storage (Burgess et al., 2013). Studies have also shown coinciding and rapid surface velocity changes that occurred after increased melt events, further proving the importance of subglacial hydrology for glacier dynamics (Zwally et al., 2002). On polythermal glaciers, long term velocity acceleration has been associated with variations in basal motion and increased hydraulic efficiency, whereas velocity decrease was likely due to a decrease in internal ice deformation and reduced basal motion (Thomson & Copland, 2017).

1.2. Glacier surging mechanisms & theories

Glacier surges describe brief periods of drastically increased velocities and high volumes of ice displacement within a glacier, driven by high overall driving stress (Cogley et al., 2011). Surge-type glaciers are glaciers which have experienced one or more surges in the past, or which contain morphological evidence of having done so (e.g., looped surface moraines). In general, each glacier surge is unique, with even repeat surges on a glacier not always consistent in duration or magnitude (Eisen et al., 2005; Main, 2024), making characterising them difficult.

The main characteristics of surging glaciers were first described by Meier & Post (1969), who emphasized the cyclicity of surging, the contrast between the much longer quiescence phase (~15-100 years), the shorter surge or active phase (typically less than 1 – 6 years on temperate glaciers),

and how the cycle duration is independent of the glaciers' characteristics and rather reliant on mass displacement. The quiescence period can be further divided into the stagnation (or depletion) phase directly after a surge with little movement, and the buildup phase, where the upper reservoir zone is actively gaining mass and the lower receiving zone is melting, with the gradient between the two zones actively growing (Jiskoot, 2011). Surge velocities can be magnitudes of order greater than those during quiescence, and the displacement of mass throughout a glacier is generally proportional to the surge velocities (Meier & Post, 1969).

There are two general categories of surge-type glaciers: Svalbard-type and Alaskan-type. Svalbard-type surge cycles are generally much longer, with active phases of up to 10 years or longer and quiescence phases of over 50 years, compared to those of Alaskan-type surges, which often have active phases of less than 2 years (Dowdeswell et al., 1991). The terms Alaskan and Svalbard do not restrict the geographical distribution of surging glaciers but denote the locations where they were first described and are most common. It is also important to note that within each category there exists a range of surge characteristics, further emphasising that no two surges are the same.

Spatial clusters of surging glaciers can be found at both a global (Sevestre & Benn, 2015; Kääb et al., 2023; Guillet et al., 2025) and regional (Clarke et al., 1986) scale. A zone titled the "Arctic Ring" encompasses a large cluster of surge-type glaciers in the Arctic and sub-Arctic from Alaska to the Russian Arctic (Sevestre & Benn, 2015), including the Yukon. The other large cluster is found in High Mountain Asia (Copland et al., 2009; Sevestre & Benn, 2015). Surge-type glaciers globally are found within a climatic envelope, with a median summer temperature of 3°C to -10°C (Guillet et al., 2025). A variety of theories and mechanisms have been explored to explain the drivers of glacier surging and why only certain glaciers experience surges. The primary theories and models for surging are outlined below.

1.2.1. Thermal instability mechanism

The thermal instability surge mechanism states that surges are initiated due to changing thermal conditions at the ice-bedrock interface for cold and polythermal glaciers. The theory is based on the principles of basal temperature and sliding (Robin, 1955), which state that ice below the pressure melting point, or "cold" ice has little to no movement between the ice and underlying bedrock. Polythermal glaciers contain a combination of cold and temperate ice (Irvine-Fynn et al.,

2011), with this ratio changing as mass accumulates on the glacier surface during the quiescent phase and the ice overburden pressure increases. As basal temperature increases due to more insulation from cold surface temperatures provided by the thickening ice, cold ice at the bed reaches the pressure melting point and once it “unfreezes”, sliding, and therefore a surge, can occur. This mechanism is suggested for slower, Svalbard-type surging glaciers, as they are not often associated with sudden terminations and water outflows indicative of basal hydrological pressure buildups (Dowdeswell et al., 1991; Murray et al., 2003). In the St. Elias Mountains, only three slowly surging glaciers which could be caused by this mechanism have been identified: Rusty, Trapridge & South (Clarke, 1976; Frappé & Clarke, 2007; Main, 2024).

1.2.2. Hydrological switch mechanism

The most explored theory for explaining glacier surging in the St. Elias Mountains is changes in subglacial hydrology. This mechanism was first described in detail for the 1982-1983 surge of Variegated Glacier, Alaska (Kamb et al., 1985; Kamb, 1987). During quiescence, a channelized subglacial hydrological system exists beneath the glacier, with low pressure tunnels kept open due to frictional heating of flowing water (Röthlisberger, 1972). As glacier thickness increases during quiescence, the overburden pressure from the overlying ice increases, until the subglacial channels can no longer stay open and instead switch to a high pressure distributed drainage system, which initiates basal sliding and therefore surging. Boreholes drilled during the surge of Variegated Glacier indicate that basal sliding and glacier velocity increased in connection with changes in subglacial water pressure, with surge initiation likely to occur when basal water pressure is consistently within 4 or 5 bars of ice overburden pressure (Kamb et al., 1985). The channelized subglacial drainage system has significantly lower water pressure than the distributed system, resulting in lower basal shear stress at the bed of the glacier during quiescence (Kamb, 1987). The distributed subglacial hydrological system allows for the high driving stress to be maintained throughout the surge (Burgess et al., 2012).

1.2.3. Pressurised till mechanism

The pressurized till mechanism (Minchew & Meyer, 2020) is a newer theory compared to the other surge mechanisms (hydrological switch and thermal switch), and is applicable to glacier surging on deformable beds. According to this model, the increase in basal sliding during surging is a result

of changing characteristics in the upper till layer which impact its shear strength, namely the ice overburden pressure, the pore water pressure and the internal friction coefficient of the till. In order for surging to occur, the till must have low hydraulic permeability and initial surge velocity must exceed the balance velocity. This requires the shear strength of the till to be less than the driving stress during quiescence. This theory differs from the hydrological switch mechanism as the till theory indicates that sliding occurs due to changing characteristics in the basal till layer, rather than the hydrological system underneath the glacier.

1.2.4. Enthalpy balance theory

The enthalpy balance theory (Benn et al., 2019a, 2019b, 2022) was created as an attempt to describe the cause of all glacier surges regardless of glacier type or mechanism. The model builds on previous findings that surge-type glaciers typically exist within a distinct climatic envelope, which may be linked to their enthalpy and mass changes based on their location (Sevestre & Benn, 2015). The enthalpy levels in the basal zone will define if a glacier is in a stable steady state (non-surging) or non-steady state (surge probable). The two main determining factors in the model are ice thickness and basal enthalpy. Basal enthalpy is impacted by the quantity of meltwater that reaches the subglacial environment, making the hydrological inputs a key factor in the model. The theory is supported by newer research evaluating surges at a global scale, which emphasizes the enthalpy balance theory to describe a range of dynamics (Guillet et al., 2025).

The hydrological switch mechanism varies from the enthalpy balance theory because in the enthalpy theory the hydrological switch occurs during quiescence and does not directly result in a surge, but instead acts as a precondition for the surge to occur (Benn et al., 2022). This slightly contradicts the hydrological switch theory as the mechanism describes the surge initiation as a direct result of the change in the basal hydrological system (Kamb et al., 1985).

1.3 Research Objectives

The primary objective of this thesis is to enhance our understanding of the underlying mechanisms driving glacier flow by mapping changes in supraglacial hydrological features during a surge in the St. Elias Mountains, Yukon. Most current theories for glacier surging emphasize the role of water and water pressure in the subglacial system, but the evolution of the supraglacial

hydrological system and its connection to dynamics and the subglacial system during a surge remains relatively unexplored.

To assess the timing and dynamics of the most recent surge of Nàłùdäy, both hydrological characteristics, including water on the glacier surface and the quantity and location of streams and moulins, as well as ice dynamics, surface velocity, crevassing and strain, are evaluated. The 2021-2022 surge of Nàłùdäy was selected for this study due to its recent and relatively short surge phase, allowing for modern, high-resolution imagery to be used, including from optical and synthetic aperture radar (SAR) satellite sources. Products derived from air photo surveys conducted during summer fieldwork, including high resolution (~50 cm) digital elevation models (DEM) and red, green, blue (RGB) orthomosaics were also used to map changes in supraglacial features such as streams and moulins throughout the surge.

Chapter 2: Linking supraglacial hydrology and surge dynamics during the 2021-2022 surge of Nàłùdäy (Lowell Glacier), Yukon, Canada.

2.1 Introduction

The St. Elias Mountains (Alaska-Yukon) is home to a large concentration of surge-type glaciers (Sevestre & Benn, 2015), in which glaciers cycle between an active phase with a sudden and rapid increase in velocity, interspersed with a period of little to no movement called the quiescent phase (Meier & Post, 1969). Theories for the cause of surging include an imbalance in the glacier's enthalpy and mass budgets (Benn et al., 2019a), changes in subglacial hydrology (Kamb, 1987), changes in glacier basal thermal regime (Clarke, 1976), changes in subglacial sediment pressure causing till instability (Minchew & Meyer, 2020), or a combination of these mechanisms.

Currently, the dominant theories for the cause of most glacier surges in the Alaska-Yukon region are an imbalance in the glacier's enthalpy budget, changes in subglacial hydrology, and subglacial till deformation. In the enthalpy balance theory, whether a glacier is in a steady state, or non-steady state (i.e. surge probable), is dependent on the mass and enthalpy budgets of the glacier (Benn et al., 2019a). In the hydrological surge mechanism, the surge is initiated by a "switch" in subglacial hydrology from an efficient channelized system with relatively low water pressure, to a distributed system with high basal water pressure which promotes rapid ice flow (Kamb et al., 1985). This is thought to occur when increasing ice thicknesses in the glacier's reservoir zone cause the channelized subglacial system to collapse due to high overburden pressure. In the subglacial till deformation theory, the sudden increase in basal sliding is caused by the deformation of the upper till layer from an increase in pressure driven by a changing porosity of the till (Minchew & Meyer, 2020). The change is porosity can be partially attributed to changes in water pressure within the upper till layer at the glacier bed. All theories are heavily reliant on basal water pressure, and thus the amount of water available and entering the basal hydrological system from the glacier surface.

Supraglacial streams work to transport meltwater on the glacier surface, before it is transported to other glacial hydrological systems. In particular, moulins act as the primary connector between the

surface and basal hydrological systems by transporting meltwater from the surface to the interior and bed of the glacier (Chu, 2014). The distribution of supraglacial hydrological features on a glacier's surface therefore has impacts on basal water pressure and the associated magnitude and location of changes in ice motion and flow (Copland et al., 2003; Wyatt & Sharp, 2015; Smith et al., 2021), on both surge-type glaciers and non surge-type glaciers, as well as ice sheets. This connection appears to be particularly important on surge-type glaciers, where surge mechanisms, such as those described above, are driven by water pressure at the base of the glacier (Kamb, 1987; Minchew & Meyer, 2020; Benn et al., 2022).

Increased surface velocities during surge phases are often accompanied by drastic changes to the glacier surface, including extensive crevassing (Jiskoot, 2011; Leclercq et al., 2021). Supraglacial hydrological systems on non-surge type glaciers are mainly defined by glacier surface topography (Karlstrom & Yang, 2016; Yang et al., 2019). The associated surface morphology changes which occur during a surge may therefore impact the ability of the supraglacial hydrological network to transport water across the glacier surface, as crevasses open up and create more surface to bed pathways (Dunse et al., 2015). Currently, a gap exists in understanding the direct impacts of surge dynamics on the supraglacial hydrological system, and in turn what that means for overall surge mechanisms and ice flow. This research addresses this gap by analysing in detail both surge dynamics and supraglacial hydrological changes during the 2021-2022 surge of Nàłùdäy (Lowell Glacier), Yukon.

2.2 Study Area

2.2.1 St. Elias Mountains

The St. Elias Mountains (Fig. 1), found along the Alaska-Yukon border, contains the largest non-polar icefield in the world (UNESCO, n.d.). The Alaska-Western North America glaciated region accounts for 12% (86,708 km^2) of all glacier area on earth outside the ice sheets, containing a total of 27,509 glaciers (Maussion et al., 2023). Out of this total, the St. Elias Mountains contains 5039 glaciers, with 33,178 km^2 of land covered in ice (RGI Consortium, 2023). The St. Elias Mountains is home to the second largest geographic cluster of surge-type glaciers globally, second only to the Svalbard Archipelago (Sevestre & Benn, 2015). The first quantification of surging glaciers in Western North America used aerial imagery to identify 204 surging glaciers, with 136 of them in

the St. Elias Mountain range (Post, 1969). The St. Elias Mountains currently has 231 glaciers identified as surge-type, which accounts for 77% of the regions glaciated area (Main, 2024).

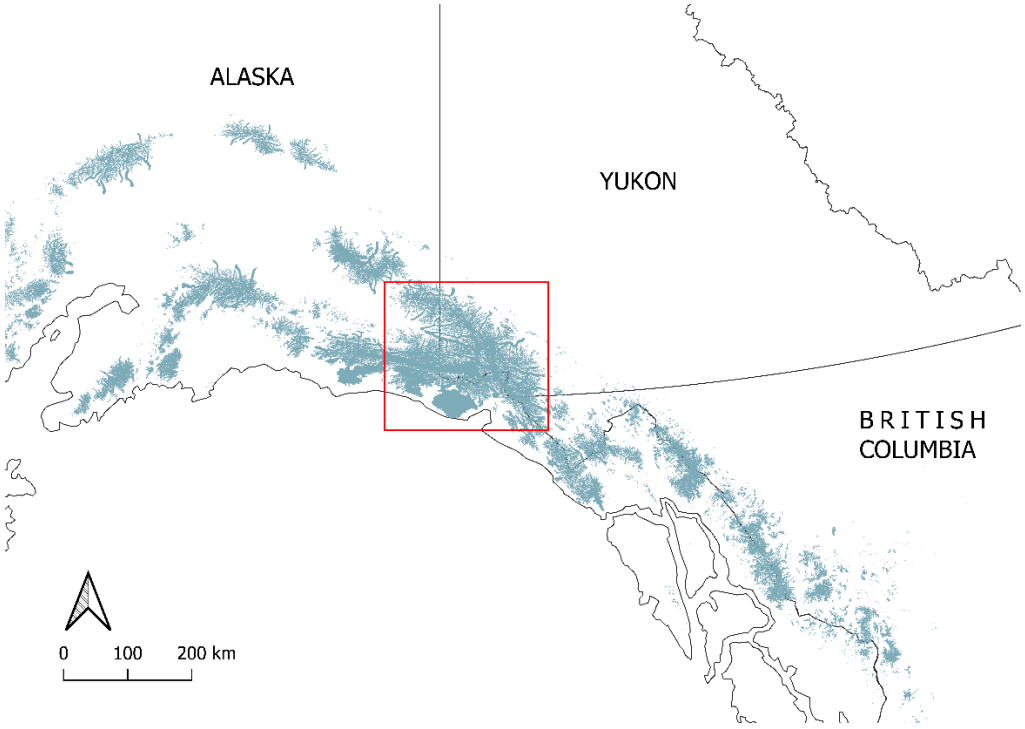

Figure 1. Map of Alaska-Western North America glaciated region (RGI 7.0) in blue with St. Elias Mountains in red rectangle.

The Alaska-Yukon region is warming at a rapid rate, with surface air temperatures increasing since 1979 at a rate of 0.019°C a^{-1} between 2000-2500 m a.s.l (Williamson et al., 2020). Between 1961 and 2016, one third of global sea level rise contributions from glacier mass change outside the ice sheets originated from the Alaska-Yukon region (Zemp et al., 2019). Over the period 2002-2019 the region's glacier mass losses averaged 72.5 ±8 Gt a^{-1}, the second highest mass loss rate of any region worldwide, only surpassed by the Canadian Arctic Archipelago (Ciracì et al., 2020). Major regional glacier mass loss is projected to continue, with the Alaska-Yukon region accounting for over 22% of the predicted 99 mm sea level equivalent (SLE) contribution from glaciers (outside ice sheets) globally by 2100 under a moderate warming scenario (+2°C; Rounce et al., 2023). The region's contribution to sea level rise in predicted to peak at 0.33-0.44 mm a^{-1} between 2030 and 2060 (Rounce et al., 2023).

Important considerations for future region-specific glacier mass loss and changes in glacier dynamics are arctic-amplified warming (AMAP, 2021; Taylor et al., 2022) and elevation-

dependent warming (EDW; Mountain Research Initiative EDW Working Group, 2015; Williamson et al., 2020). At higher elevations in mountainous regions, feedback mechanisms including albedo, cloud cover, water vapour and radiative fluxes, and aerosols, cause greater change in atmospheric temperatures than at low elevations (Mountain Research Initiative EDW Working Group, 2015; Williamson et al., 2020). The amplified warming at higher elevations in this region has been primarily linked to an increase in longwave radiation vapour feedback (Williamson et al., 2020). The combination of amplified warming rates and a large variation in glacier dynamics in the St. Elias Mountains makes understanding underlying mechanisms driving surges and their connection to supraglacial hydrology important both at a local and global scale.

2.2.2 Nàłùdäy (Lowell Glacier)

Nàłùdäy (Lowell Glacier; 60.312°N, 138.377°W) is a large valley glacier located on the southeast side of the St. Elias Mountains, with most of its ablation area on the traditional territory of Champagne and Aishihik First Nations, in Kluane National Park and Reserve. Including all its tributaries, Nàłùdäy has a total area of 583 km^2 (RGI Consortium, 2023); this study focuses on the main trunk of the glacier's ablation area, with an area of approximately 200 km^2 (Fig. 2). The main trunk flows in an approximately west to east direction and terminates in Lake Alsek, which flows into the Alsek River, before entering the Gulf of Alaska. The main accumulation region for Nàłùdäy is shared with Fisher and Hubbard Glaciers to the south and southwest, with a secondary icefall originating from an adjacent surge-type glacier to the north, Dusty Glacier (Bevington & Copland, 2014).

Environment and Climate Change Canada climate records from the nearby town of Haines Junction (approximately 65 km NNE of Nàłùdäy) shows a precipitation normal of 306 mm a^{-1} from 1991 to 2020 (Environment and Climate Change Canada, n.d.). A weather station located on a nunatak near the icefall between Nàłùdäy and Dusty Glacier (Fig. 2) recorded an average annual air temperature of -4.1°C between 2019-2023 (Partington, 2023).

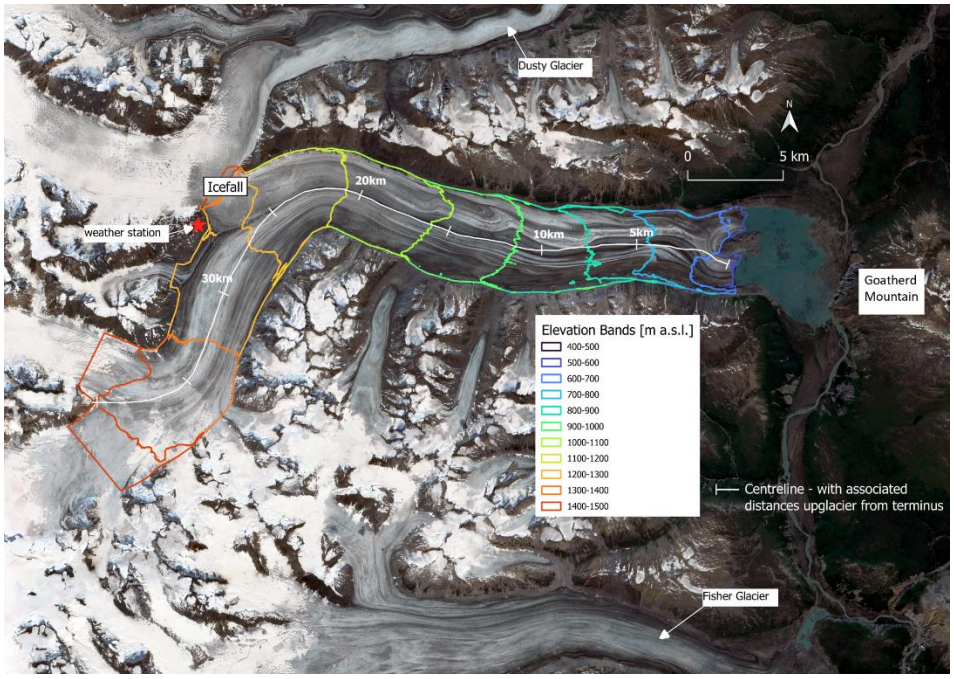

Figure 2. Map of Nàłùdäy with elevation bands clipped to the study area outline. Base image Sentinel-2 Q3-2024 cloud free mosaic, with elevation bands from ArcticDEM 2 m Mosaics v4.1. Nearby glaciers Dusty and Fisher are also identified, as well as the shared icefall with Dusty Glacier. White line with 5 km markers indicates distance upglacier from terminus along centre flowline.

Nàłùdäy has surged 6 times since the late 1940s, with active phases in 1948-50, 1968-70, 1983-84, 1997-98, 2009-10 and 2021-22 (Bevington & Copland, 2014; Van Wychen et al., 2023). Surges at Nàłùdäy are identified by surface velocity increases by up to two orders of magnitude (Van Wychen et al., 2023), rapid terminus advance of up to several km (Bevington & Copland, 2014), and dramatic increases in crevassing. Studies indicate that neoglacial Lake Alsek formed multiple times during historical surges when the glacier dammed the Alsek River by extending to Goatherd Mountain (Clague & Rampton, 1982), resulting in large downstream floods when it drained (Cruikshank, 2001).

SAR derived velocities indicate that the most recent surge of Nàłùdäy initiated near the terminus, and progressed upglacier, with surge velocities present in January 2022 (Van Wychen et al., 2023). The surge initiated after an approximately 11-year quiescent period following the 2009-2010 surge (Bevington & Copland, 2014; Van Wychen et al., 2023). The 2021-2022 surge had a significant impact on the glacier surface (Fig. 3), with extensive crevassing across the lower portion of the glacier and advance of the terminus by up to ~1.7 km on the south side of the nunatak into Lake Alsek.

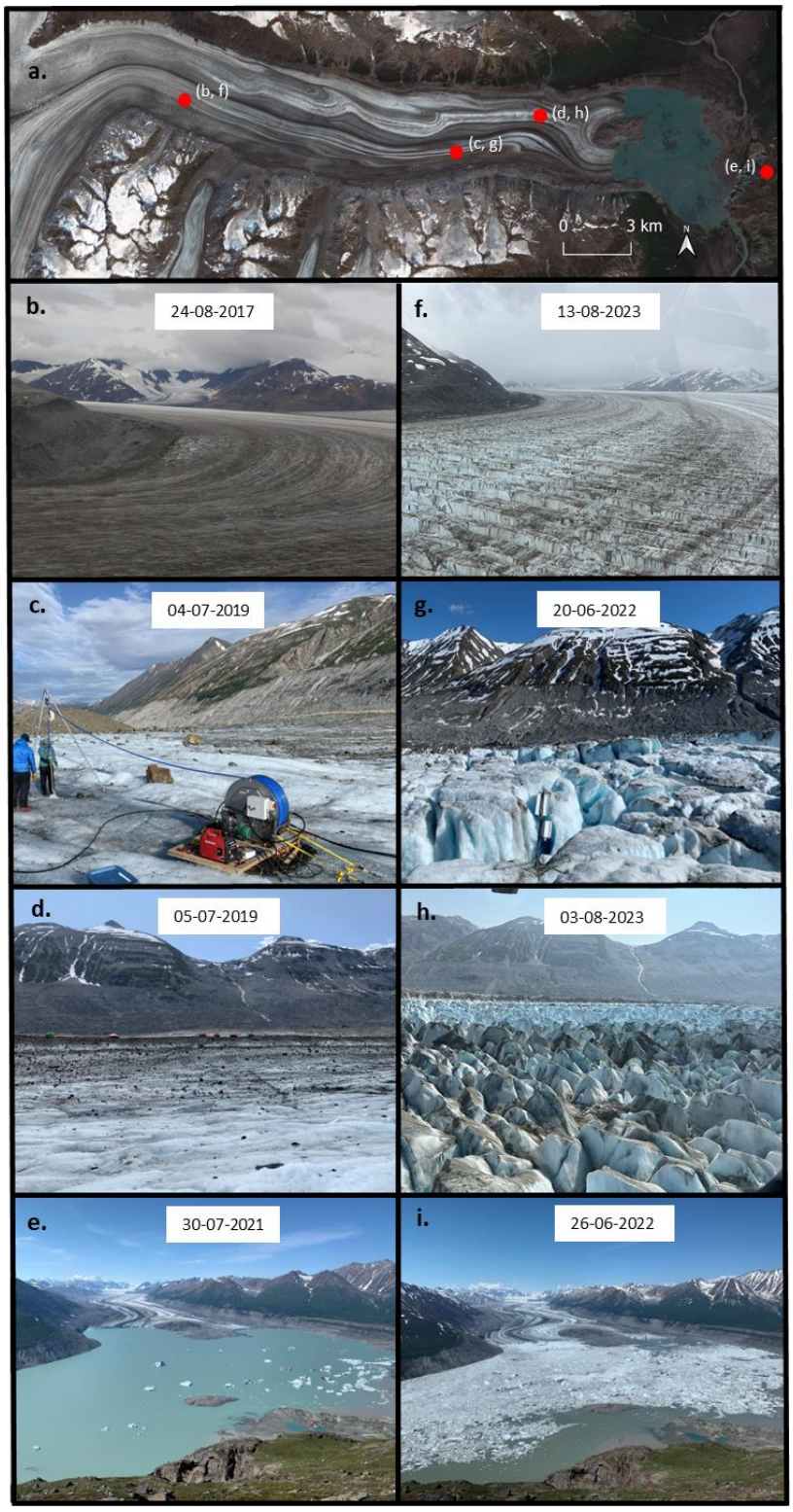

Figure 3. Images taken at similar locations from before and during/after the 2021-2022 surge of Nàłùdäy with a map (a) showing approximate photo locations. Photos were taken near the upper corner (b, f), south arm (c, g), north arm (d, h), and from Goatherd Mountain overlooking the terminus (e, i).

2.3 Methods

2.3.1 Surface hydrological changes

2.3.1.1 Surface hydrology mapping

To assess changes in hydrology during the 2021-2022 surge of Nàlùdäy compared to conditions before and after the surge, the first step was to determine the amount of water on the glacier surface at a given point in time. Orthorectified multispectral Sentinel-2 surface reflectance imagery (Level-2A, Collection 1) from the European Space Agency was used for this (accessed using https://dataspace.copernicus.eu/browser/). One cloud-free and snow-free image was selected for each summer period (mid-July to mid-August) from 2020 to 2024, with the required multispectral bands having a resolution of 10 m (Table 1).

Table 1. Satellite imagery used for surface water detection on Nàlùdäy from 2020 to 2024.

Acquisition Date [dd-mm-yyyy]	**Image ID**	**Satellite**
16-07-2020	S2A_MSIL2A_20200716T204021_N0500_R014_T07VFG_20230515T193614	Sentinel-2A
31-07-2021	S2A_MSIL2A_20210731T204021_N0500_R014_T07VFG_20230121T032907	Sentinel-2A
12-08-2022	S2A_MSIL2A_20220812T202901_N0400_R114_T07VFG_20220813T031902	Sentinel-2A
28-07-2023	S2A_MSIL2A_20230728T202851_N0509_R114_T07VFG_20230729T015000	Sentinel-2A
06-08-2024	S2B_MSIL2A_20240806T202849_N0511_R114_T07VFG_20240807T003749	Sentinel-2B

A modified Normalised Difference Water Index (NDWI) was used to enhance water pixels on the glacier surface. The standard NDWI utilises variations in reflectance of the near-infrared and green bands to enhance water on vegetated surfaces (McFeeters, 1996). This index has been modified to define water on ice surfaces, rather than vegetation, by contrasting the reflectance in the blue and red spectral bands (bands 2 and 4 for Sentinel-2 imagery) in the Normalised Difference Water Index for Ice ($NDWI_{ice}$) (Yang & Smith, 2012):

$$NDWI_{ice} = \frac{blue-red}{blue+red} \quad (1)$$

Once the modified $NDWI_{ice}$ was created, a threshold was used to determine if water was present on the glacier surface. The threshold was defined based on comparison with true colour imagery, as well as analysis of histograms of the $NDWI_{ice}$ value range. This showed that water was present on the glacier surface with high confidence when water pixels had an $NDWI_{ice}$ value of >0.18.

2.3.1.2 Stream & moulin mapping

Supraglacial streams and moulins were identified using orthomosaics derived from air photos taken during piloted structure from motion (SfM) surveys during field campaigns in summer 2019 and summer 2023 (Table 2). These surveys were performed using a Nikon D850 SLR 46-megapixel camera, mounted through the floor of a fixed wing Helio Courier aircraft, and set to take photos every 3 seconds (~2000-3000 photos per survey). Surveys included 6 longitudinal lines parallel to the centreline of Nàłùdäy at an approximate height of 500 m above ground level. Images were aligned using corresponding multi-frequency Global Navigation Satellite System (GNSS) locations recorded with a Trimble R7 (in 2019) or Emlid Reach M2 (in 2023) receiver, which ran simultaneously with a base station installed on bedrock adjacent to the weather station at Nàłùdäy (Fig. 2). Processing was undertaken using Agisoft Metashape Professional 2.0.3, following the procedures described in Medrzycka (2022) and Medrzycka et al. (2025). Tie points were first used to create a sparse point cloud, followed by a dense point cloud. This dense point cloud was then processed to create a digital elevation model (DEM) and orthomosaics, both with a resolution of less than 0.5 m.

Table 2. Processing statistics for SfM air photo surveys of Nàłùdäy using Agisoft Metashape 2.0.3.

Survey date [dd-mm-yyyy]	**Number of images**	**Ground resolution - orthomosaic [cm]**	**DEM resolution [cm]**	**Number of tie points**	**Reprojection Error [pixels]**
01-07-2019	2 662	22.7	45.4	17,426,725	0.629
06-08-2023	2 031	19.8	39.5	1,261,953	1.07

A 500 m x 500 m grid was overlaid on the orthomosaics and used as a search viewing window to manually identify surface streams at an average scale of 1:800. Visible streams were manually digitised as shapefile line segments, and where uncertainty occurred an $NDWI_{ice}$ index of the orthomosaics was created using the red and blue bands in the air photos to determine if water was present on the glacier surface. When streams were identified, they were mapped and followed

upglacier until the stream was no longer identifiable. Moulins were identified as streams that abruptly terminated in dark, circular shapes, that did not specifically contain water pixels. Moulins with no water input (i.e., previous moulin or a hole in the glacier) were not mapped.

2.3.2 Surge progression mapping

2.3.2.1 Crevasse extent

Backscatter from synthetic aperture radar (SAR) images has been previously used to identify increased roughness on the glacier surface attributed to crevassing caused by surging (Abe & Furuya, 2015; Leclercq et al., 2021; Kääb et al., 2023; Guillet et al., 2025). In this study, crevasse extent was mapped using Sentinel-1 C-band SAR ground range detection (GRD) imagery from 2020 to 2024, to assess the evolution of crevassing throughout the most recent surge of Nàłùdäy. Crevasse extent was analysed using Google Earth Engine, using methodologies developed in Leclerq et al. (2021). Winter crevassing maximums were created by stacking all available ascending orbit, VH polarization imagery from January 1 to April 30 in each year (Table 3). Ascending orbit scenes were chosen due to the greater availability of images in the study region compared to descending orbit, which stopped being acquired with the failure of Sentinel 1B in late 2021. A composite was created from the maximum pixel value for each pixel within the stack, which were clipped to the study area's extent (Fig. 2). The resulting winter maximum composites are assumed to represent the maximum crevassed area reached during each winter period.

Table 3. Number of Sentinel-1, ascending orbit images used in the creation of annual mosaics in Google Earth Engine from 2020 to 2024 for crevasse detection. Details of individual images used to create each annual stack can be found in Table A-1.

Year	Number of ascending images
2020	18
2021	19
2022	7
2023	3
2024	5

A threshold value to identify crevassing was then determined by comparing backscatter intensity values from the winter annual maximum imagery to early summer high resolution optical imagery from the same year to find the best value to define an area as crevassed. For Sentinel-1 imagery a

value of -12.0 dB was selected, with values greater than the threshold being marked as crevassed areas. A binary raster of crevasse or crevasse-free glacier surface was then created.

2.3.2.2 Surface velocities & longitudinal strain rate calculations

This study used ice surface velocities from the NASA Inter-mission Time Series of Land Ice Velocity and Elevation (ITS_LIVE) (Gardner et al., 2025) project through its website https://its-live.jpl.nasa.gov/. All available regional annual velocity mosaics for the Alaska and Western North America (ALA) region, with a resolution of 120 m, were downloaded and clipped to the glacier outline of Nàłùdäy. The annual mosaics were created using the error-weighted average of all the individual image pairs collected within the year, generated using automated feature tracking (auto_RIFT v1).

Individual image pairs from ITS_LIVE between June 2020 and February 2023 were also evaluated to examine shorter-term velocity changes during the surge. Image pairs with time separation between images of 7 to 45 days were selected to quantify short-term patterns and filtered to ensure that the error values were less than 50% of the velocity magnitude.

Long-term longitudinal surface strain rates for Nàłùdäy were calculated from the variation in surface velocity over a defined distance, following the methodology of Alley et al. (2018) and Van Wychen et al. (2025). The longitudinal surface strain rate was computed using NASA ITS_LIVE regional annual velocity mosaics from 1984 to 2022 (Gardner et al., 2025). Three flowlines along Nàłùdäy were used: North, Central and South (Fig. 4). Velocities were sampled at 1000 m intervals along the three flowlines to calculate strain rates using the equation:

$$Longitudinal\ surface\ strain\ rate = \frac{du}{dx} = \frac{u_2 - u_1}{dx} \quad (2)$$

Where *du* is the difference in velocity between two points in the upglacier direction, and *dx* represents the distance between the two points. Strain rate was calculated in the upglacier direction, so a positive strain rate shows a surface acceleration, or extension, and a negative strain rate represents surface deceleration, or compression (Cuffey & Paterson, 2010). Resulting longitudinal strain rate values were assigned the location of the centre point along the flowline between the two sampled velocities, then averaged per 100 m elevation band (Fig. 4). For consistency, all years used elevation bands of Nàłùdäy created from ArcticDEM mosaics (v4.1), cropped to the glacier outline from RGI 7.0 (source date August 14, 2010).

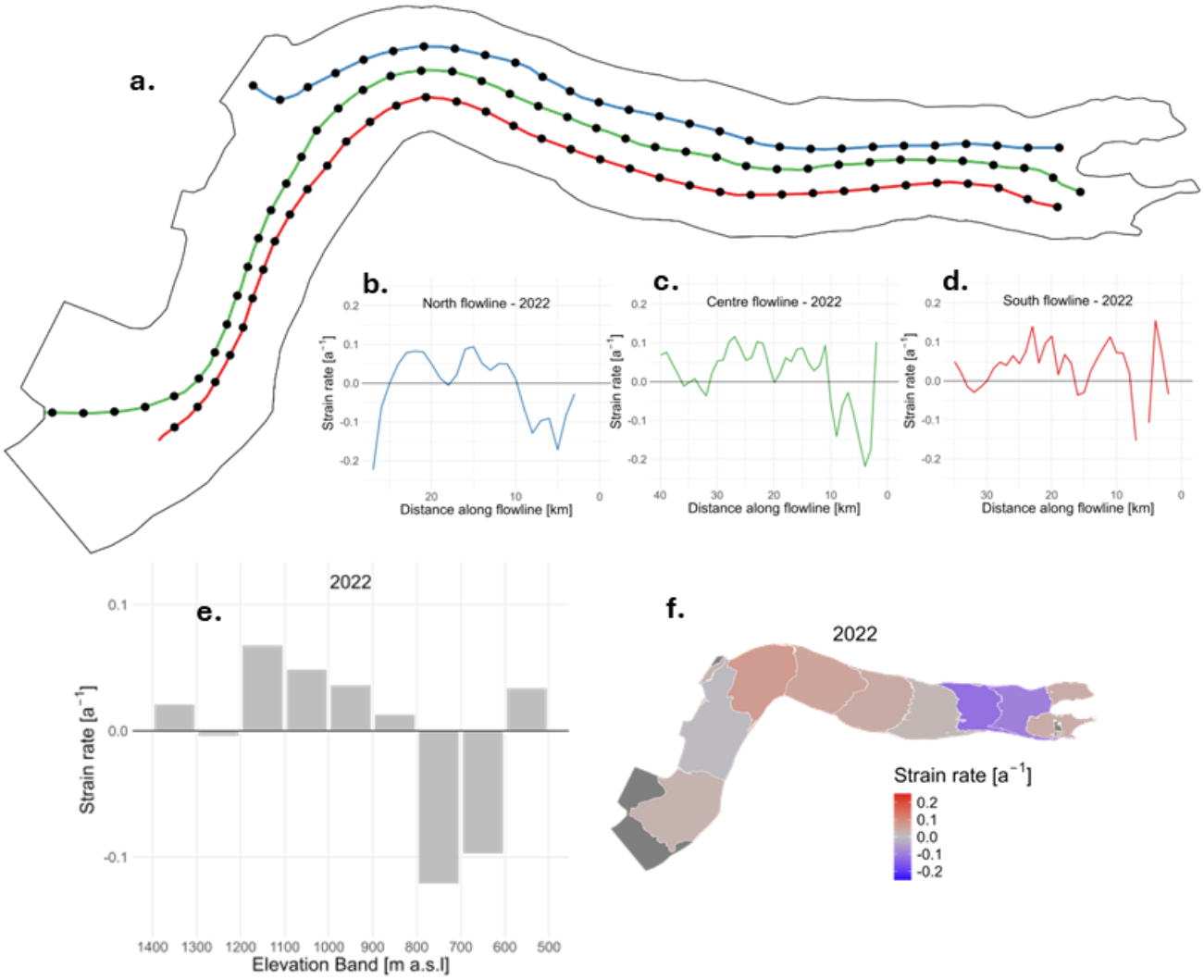

Figure 4. (a) North (blue), central (green) and south (red) flowlines used for surface strain rate calculations. Resulting strain rate for 2022 along: (b) north, (c) central, and (d) south flowlines. (e) and (f) average strain rate per 100 m elevation band for 2022. Positive strain rate values indicate extension, negative values indicate compression.

2.4 Results

2.4.1 Supraglacial hydrology

2.4.1.1 Surface water changes

To assess changes in surface hydrology on Nàłùdäy, pixels of water defined from the $NDWI_{ice}$ index were compared annually from 2020 to 2024. The total water on the glacier surface remained relatively low for 2020 and 2021, before increasing in 2022. In 2020, a large volume of water was held in a supraglacial lake in the 1300-1400 m elevation band, near the upper region of the study

area (Fig. 5). The lake was at it's largest in mid-July 2020, with a water area of 0.147 km^2 (Fig. 6b). From optical image observations the lake had partially drained by August 3, 2020 and was fully empty on August 11, 2020. No other supraglacial lakes were identified on Nàłùdäy during the study period (2020-2024), and optical imagery indicated that none were present in 2019 either.

In 2020, when the area of the upper supraglacial lake is removed, there was 0.0054 km^2 of water on the glacier surface, almost all of it concentrated above 800 m elevation (Fig. 5). In July 2021, the total amount of water on the glacier surface was 0.0114 km^2, with 78.1% of that between 1200-1400 m a.s.l. From summer 2021 to summer 2022, the total water on the glacier surface increased by almost 3 times, from 0.0114 km^2 to 0.0331 km^2, with pronounced increases in all elevation bands up to 1200 m. In July 2023, there was a slight decrease in surface water, to 0.0280 km^2 across the entire glacier, followed by a drastic increase to 0.0764 km^2 in 2024. In 2024, there is a large concentration of water pixels found from 900 m to 1200 m a.s.l., with 75.8% of such pixels found in this region; this area is located slightly downglacier of the icefall, which enters Nàłùdäy in the 1200-1300 m elevation band.

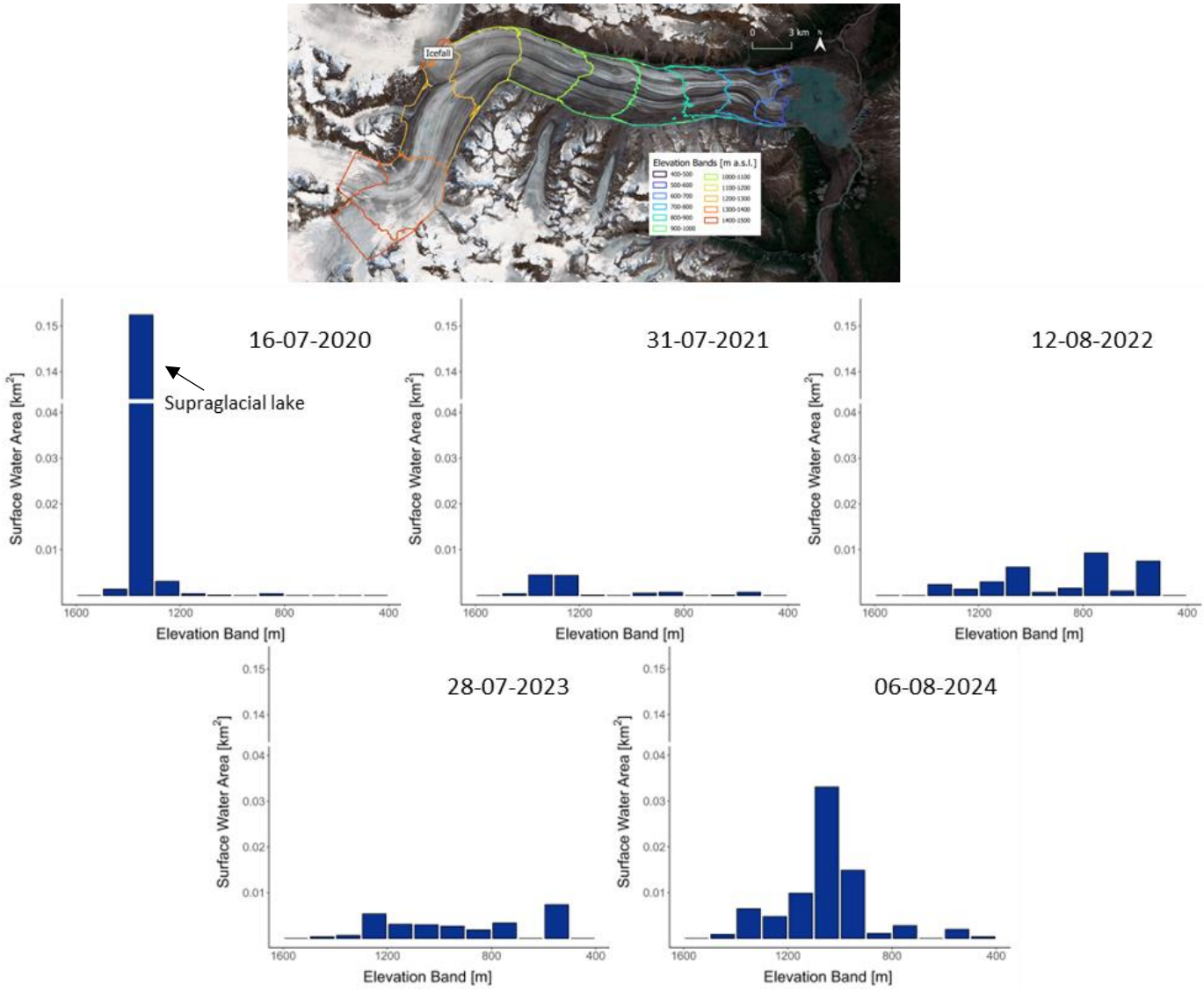

Figure 5. Surface water area of Nàłùdäy derived from Sentinel-2 imagery from 2020 to 2024 by elevation band which contains water (NDWIice > 0.18). Note break in y-axis (Xu et al., 2021) to show area of supraglacial lake in 2020.

Analysis of true colour Sentinel-2 imagery was used to investigate how the water is stored on the glacier surface. As discussed above, most water pixels in summer 2020 are concentrated in a lake in the upper part of the glacier (Fig. 6a, b). In contrast, water pixels in the year with the next largest water area, 2024, mainly occur in crevasses (Fig. 6c). These crevasses are distinguished in optical imagery as cracks that are typically oriented perpendicular to the glacier flow direction, with blue water in them (Fig. 6d, e, f).

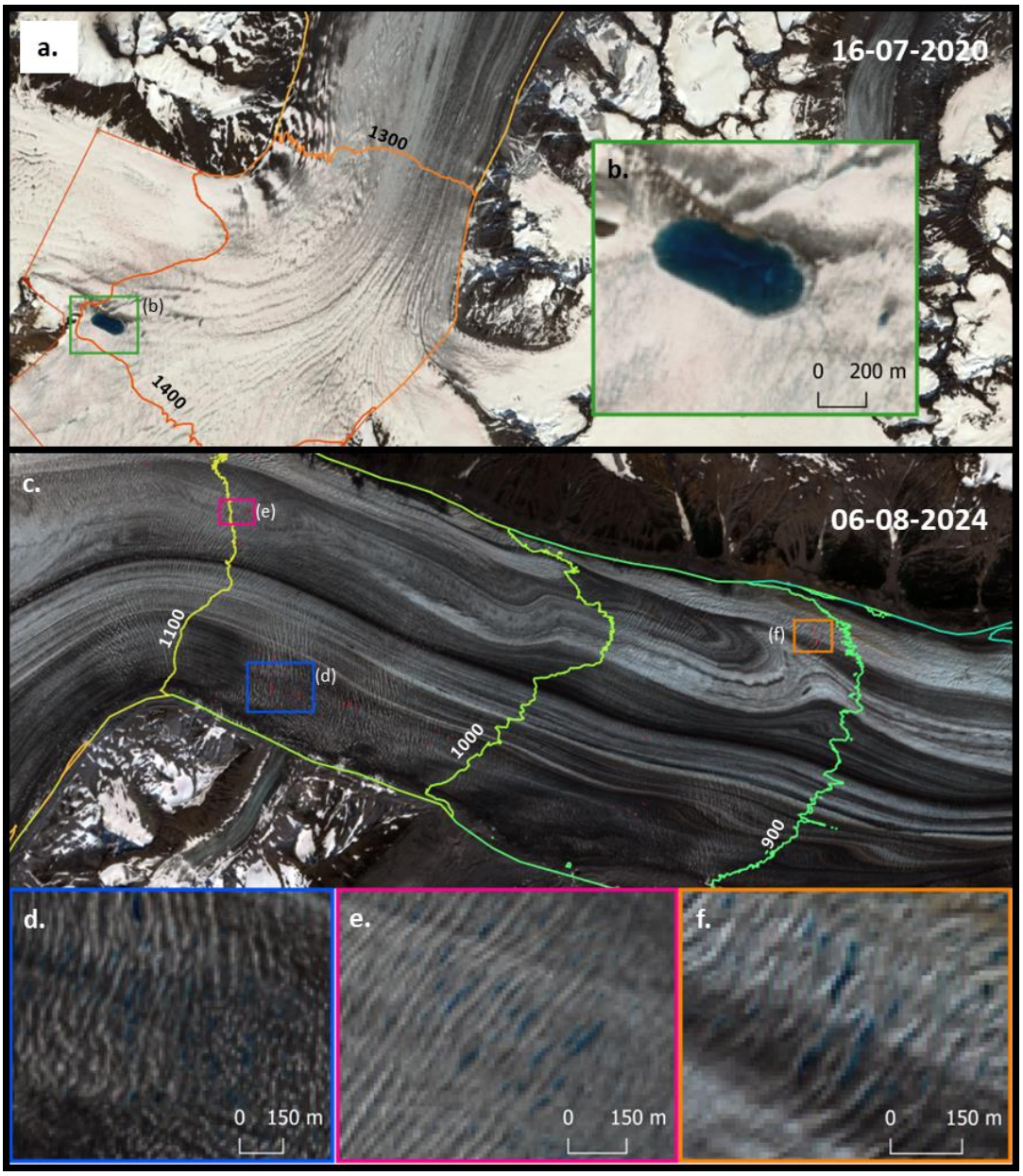

Figure 6. (a) Map of upper Nàlùdäy in summer 2020, showing supraglacial lake with water pixels (red), and (b) zoomed in Sentinel-2 imagery of the lake. (c) Map of water pixels (red) on Sentinel-2 imagery from summer 2024 showing (d, e, f) water filled crevasses. Coloured lines on (c) show surface elevation contours in m a.sl.

2.4.1.2 Supraglacial drainage network changes

Supraglacial drainage features including streams, moulins and collapse features were mapped for summer 2019 and summer 2023 from the high resolution air photo orthomosaics before and after the surge of Nàlùdäy (Fig. 7). In 2019 the images were acquired about a month earlier than in 2023, so snow still covered the upper part of the study area (snowline ranged from 1194 to 1307

m a.s.l.), making it more difficult to reliably map features in this upper elevation region than in 2023 when the glacier surface in the study area was fully snow-free.

In 2019 supraglacial streams were common over most parts of the glacier, with a total length of 200.77 km (Fig. 7a). In 2023 the stream network was noticeably less extensive, with a length of 93.05 km, a decrease of 53.7% from pre- to post-surge (Fig. 7b). The corresponding total drainage density decreased from 1.05 km km^{-2} in 2019 to 0.48 km km^{-2} in 2023. Prior to the surge initiation, in July 2019, the largest concentration of streams by length was found in the 1200-1300 m elevation band, with 66.4% of the total above 1000 m a.s.l (Fig. 8a). In this year the stream system was dominated by clusters of small dendritic networks that fed into each other and often terminated in moulins.

Summer 2023 shows a more fragmented and less extensive stream system on the surface of Nàłùdäy; of the 93.05 km of supraglacial streams present, 67.1% were located between 800 and 1200 m a.s.l. The highest drainage density in 2023 was 0.84 km km^{-2} and 0.82 km km^{-2}, found in the 800-900 m and 1100-1200 m elevation bands, respectively. These values are 47.7% and 50.0% lower than the 2019 drainage density at the same elevation. The 2023 stream system was comprised of smaller segmented streams, many of them running perpendicular to glacier flow.

Over the entire study period, stream length and drainage density was lowest in the 500-600 m elevation band, with a density of only 0.03 km km^{-2} in 2019 and no streams in 2023. Overall, both prior- and post-surge the highest drainage density was found at the 800-900 m and 1100-1200 m elevation bands.

Two collapse features (Fig. A-1) were identified in 2019, one on the north arm approximately 3.8 km upglacier from the north arm terminus, at around 619 m a.s.l., and another along the south arm approximately 4.8 km above the south arm terminus at 690 m a.s.l. The collapse features present

as circular crevassing around a central sinkpoint, forming a general depression around the center, with an approximate diameter of 150 m. No collapse features were identifiable in 2023.

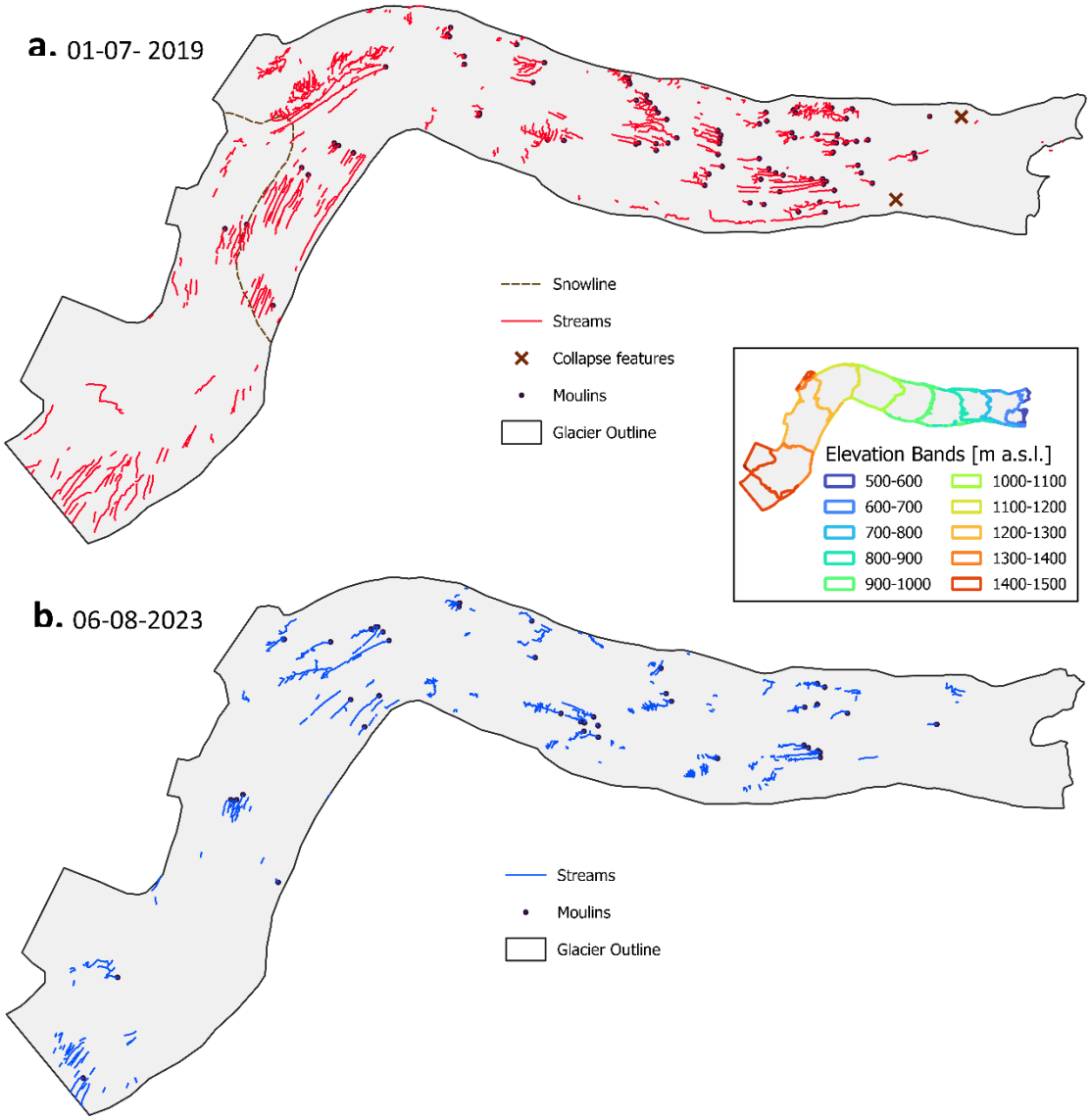

Figure 7. Supraglacial drainage network changes mapped from SfM air photo surveys in: (a) summer 2019, (b) summer 2023.

In July 2019, 91 moulins were mapped on the glacier, all from 600 m a.s.l. to 1300 m a.s.l., with 87.9% of them clustered between 700 to 1000 m a.s.l. (Fig. 8a). The total moulin count decreased by 51.7% from 2019 to 2023, to 44 moulins over the entire glacier in summer 2023. The number of moulins decreased at bands below 1100 m a.s.l., but increased above 1100 m a.s.l. and were

identified further upglacier in 2023 than 2019, although this could be due to the higher possibility of errors of omission above the snowline in 2019. In both 2019 and 2023, moulins were spatially distributed across both the north and south arms of Nàłùdäy.

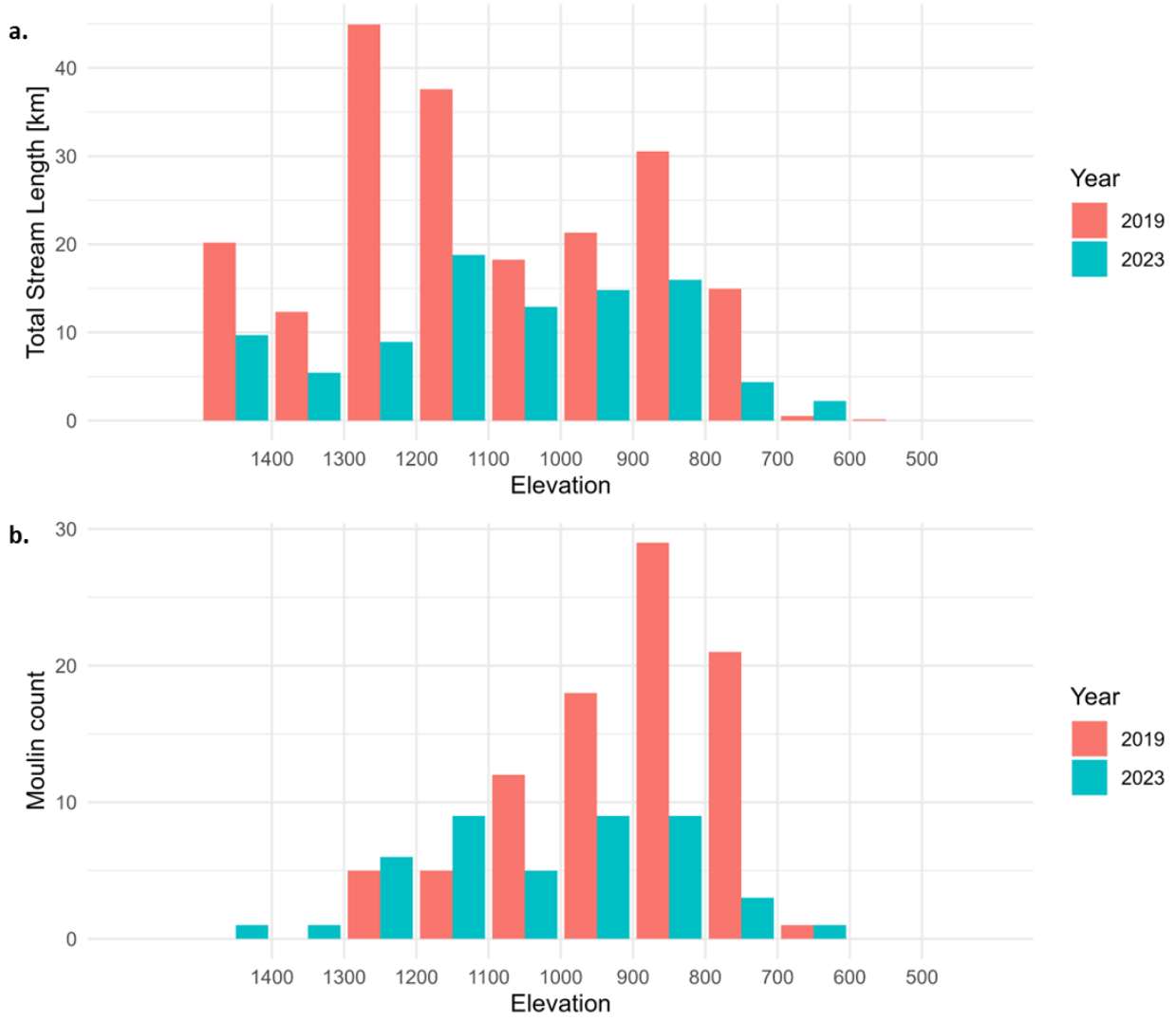

Figure 8. (a) Total stream length [km] and (b) moulin count per elevation band in summer 2019 and 2023.

2.4.2 Crevasse changes

Nàłùdäy experienced a gradual upglacier expansion of crevassing during the most recent surge (Fig. 9). From 2020 to 2023 crevassing gradually increased at nearly every elevation band up to 1300 m. Above this, crevassing remained relatively consistent, with less than 1% variability between years (Fig. 10). In 2024, crevassing began to decrease across most of the glacier, with the exception of a slight increase from 4.9% to 7.1% in the 1300-1400 m elevation band. Maximum

crevassing occurred in winter 2023, when 29.0% of the entire glacier was crevassed. Prior to surge initiation, 9.0% of the glacier surface was crevassed in 2020, and 14.2% in 2021.

During peak crevassing, the majority of the crevassed pixels were found below 1000 m a.s.l., with 51.8% of the glacier surface below 1000 m crevassed in 2023, an increase from 39.8% in 2022 and 25.6% in 2021. Above 1000 m a.s.l., changes in crevassing over time were less significant, ranging from 6.4% in 2021, to 8.5% in 2022, 14.1% in 2023 and 11.4% in 2024. In the 1200-1300 m elevation band, where the icefall joins Nàłùdäy, crevassing remained consistent with values ranging from 12.4% to 13.2% from 2022 to 2024.

Crevassing along the glacier margins was present in all study years, although it increased each year from 2020 to 2023, followed by a decline in 2024 (Fig. 9). In 2022, most of the north margin was covered in crevasses, with the south margin only being partially covered. The south margin did not become fully crevassed until winter 2023.

Prior to surge initiation, there was an increase in crevassing near the south arm of the terminus in winter 2021 (Fig. 9). Further analysis of individual SAR scenes from this winter period (Fig. A-2) showed a terminus calving event that took place between January 17 and January 29, 2021. This event can be seen by an increase in backscatter along the south arm terminus after January 29, 2021. Optical imagery from May 2021 shows broken up ice near the south terminus. By June 8, 2021, all remaining broken pieces of ice have drifted away from the terminus and are found near the east side of Lake Alsek, opposite the terminus of Nàłùdäy.

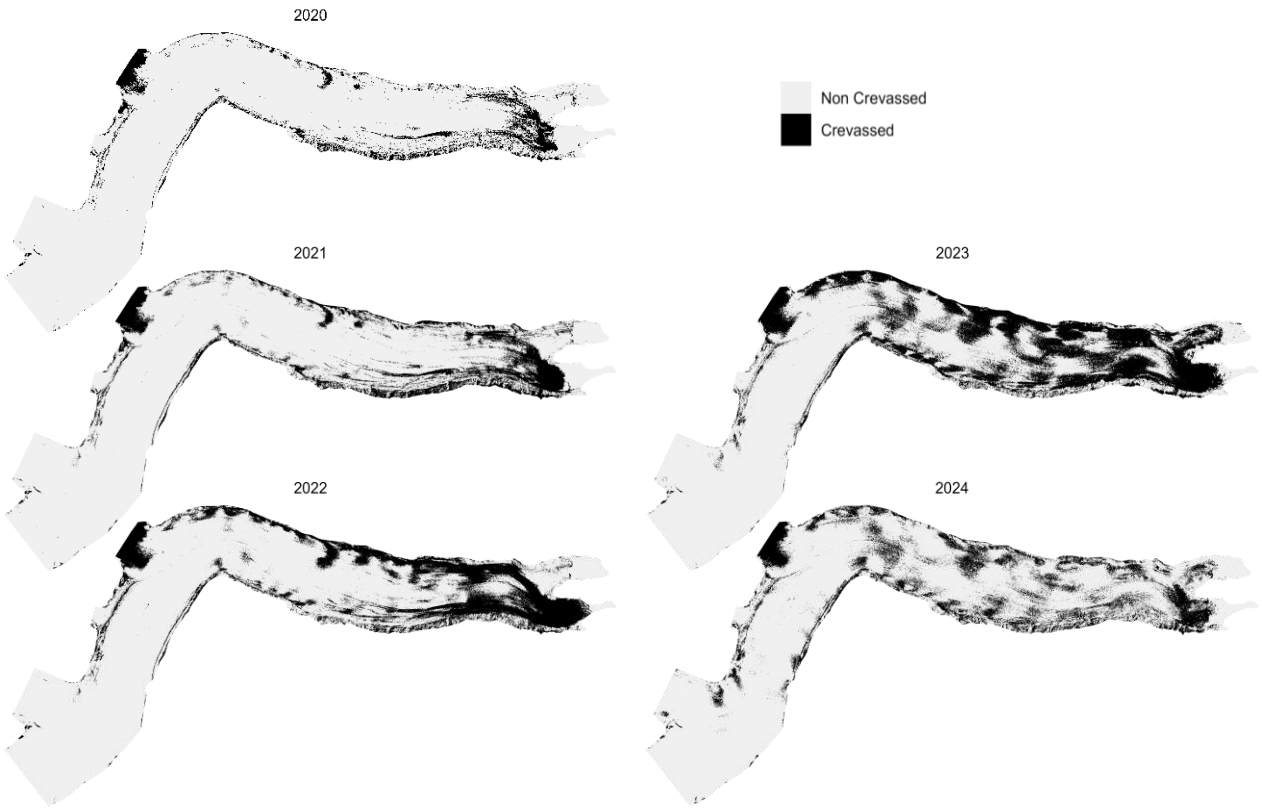

Figure 9. Crevassing extent from 2020 to 2024 showing surge progression of Nàłùdäy derived from annual winter maximum backscatter values from Sentinel-1 imagery.

The elevation band containing peak crevassing extent migrated upglacier during the surge, coincident with increases in the amount of crevassing within that band (Fig. 10). In winters 2020 and 2021, prior to surge initiation, peak crevassing occurred in the 600-700 m band. As the surge progressed, this peak migrated upglacier to the 700-800 m band in 2022 and 2023. In 2024, after the surge has terminated and Nàłùdäy has returned to a quiescent period, there is no distinguishable peak crevassing point along the glacier.

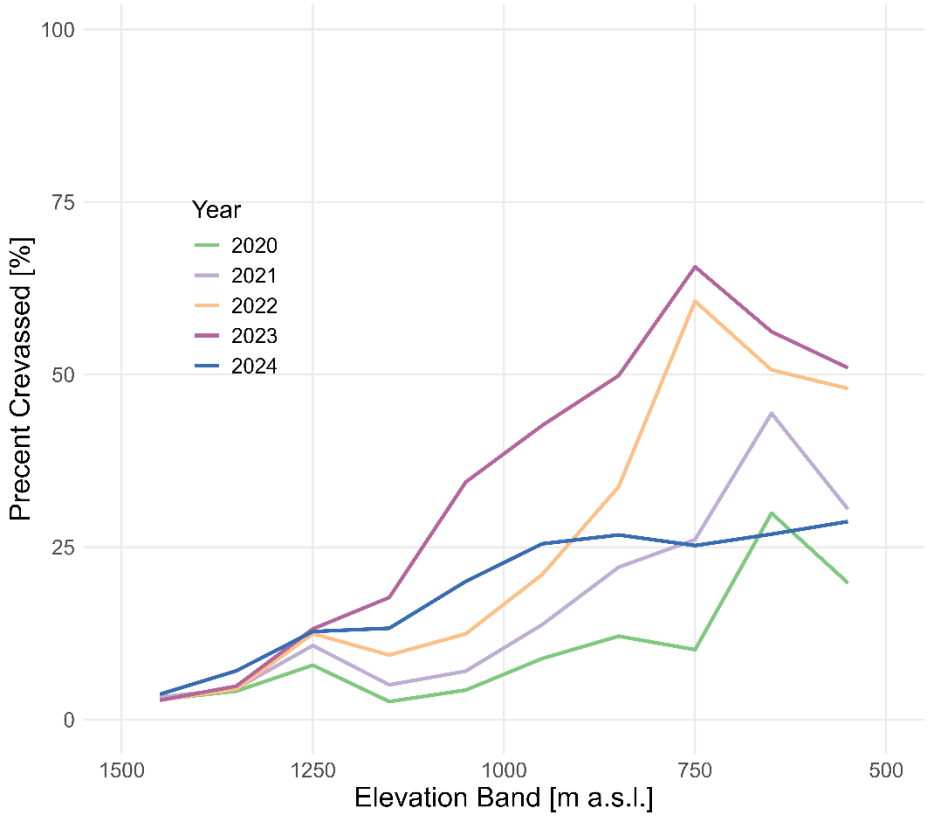

Figure 10. Percent crevassing by elevation band from annual winter maximum backscatter composites using defined crevassing threshold (-12.0 dB) from 2020 to 2024.

2.4.3 Dynamic changes

2.4.3.1 Velocity changes

NASA ITS_LIVE annual velocity mosaics provide information about the characteristics of the previous three surges of Nàłùdäy (Fig. 11). Annual velocities appear to be faster during the most recent surge (2021-2022), although this may also be due to the greater availability and resolution of satellite imagery towards present day. Peak velocities during the 2021-2022 surge from the annual mosaics were 1549 m a^{-1} in 2022 at 9 km upglacier from the terminus. In comparison, the peak for the 1997-1998 surge occurred in a similar location at ~9 km upglacier at 1225 m a^{-1} in 1997 (although a data gap below 7 km exists in 1997), whereas the peak for the 2009-2010 surge occurred at 24 km upglacier at 910 m a^{-1} in 2010.

In all velocity profiles, during both quiescence and active surge phases, there is a region of higher velocities at ~25 km upglacier from the terminus. This represents the location where the icefall

enters Nàłùdäy. The enhanced velocities occur until ~8-12 km downglacier from the icefall, when they drop considerably, to less than 150 m a^{-1} during quiescent phases.

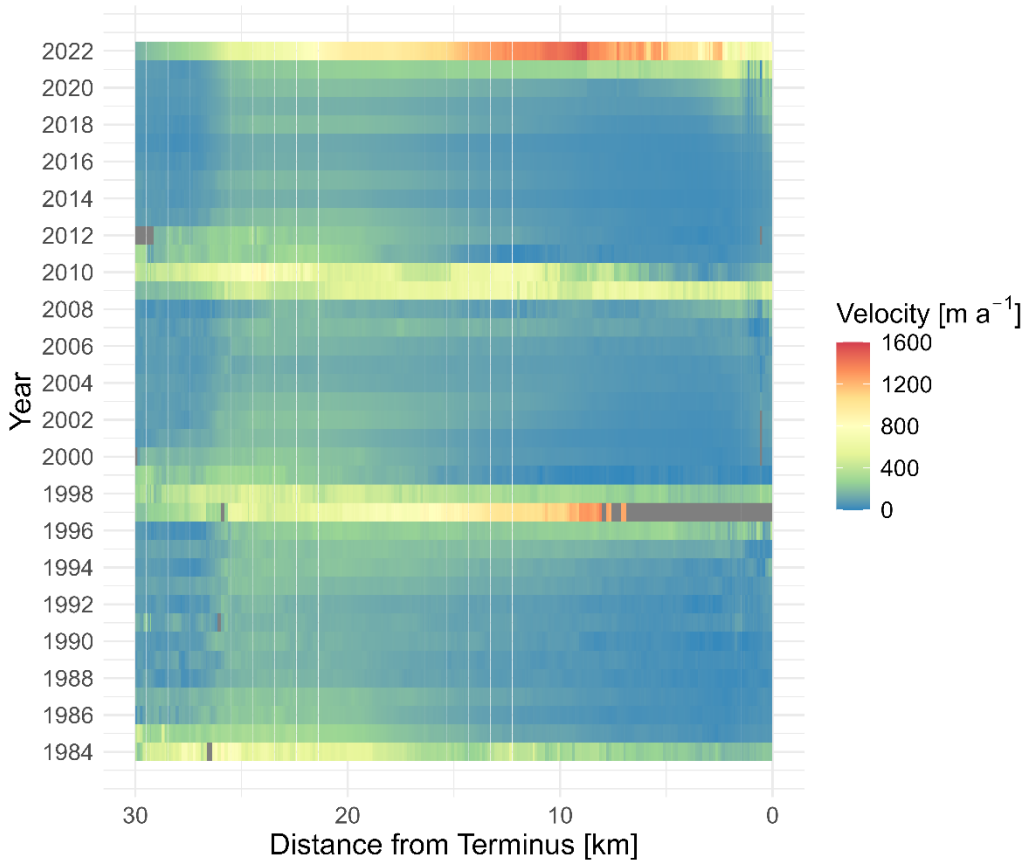

Figure 11. Annual velocity mosaics from NASA ITS_LIVE project, extracted along the centreline (Fig. 2) of Nàłùdäy from 1984 to 2022.

A more detailed understanding of how velocities evolved throughout the most recent surge is provided by data from individual image pairs (Fig. 12). Velocities first increased near the south arm of the terminus around May 2021, from a consistent ~500 m a^{-1} (similar to values during quiescence), to slightly over 1000 m a^{-1} by mid-June 2021. The south arm terminus velocity then remained around 1000 m a^{-1} until fall 2021. Points along the north arm experienced an increase in velocities at a similar timing to those of the south arm in spring 2021, from ~100-200 m a^{-1} to 500-600 m a^{-1} around 5 km upglacier from the terminus. Velocity increases also occurred at points further upglacier along the north arm at this time, but to a lesser degree.

After the initial spring 2021 acceleration, in November 2021 velocities began to increase rapidly at approximately 5 km upglacier from the terminus along the north arm (Fig. 12b). Velocity

increases followed at locations further upglacier along the north arm and south arm, and downglacier along the south arm. Peak velocities occurred in spring 2022, at approximately 5 km upglacier from the terminus along the north arm, reaching 4263 +/- 97 m a^{-1} on a mid-date of April 13, 2022. Comparatively, peak velocities along the south arm were lower, reaching 2397 +/- 52 m a^{-1} near the terminus in June 2022.

Velocity changes clearly propagated in an upglacier and downglacier direction. Along the north arm, velocities first increased around 5 km upglacier from the terminus, then propagated upglacier until near the icefall, around 25 km upglacier. As the velocities progressed upglacier they reduced in magnitude. Below the 5 km mark the north arm terminus had an initial, small acceleration in late fall 2021, which reduced in winter 2022, followed by a pronounced acceleration in spring 2022, with the highest recorded values of 1149 +/- 33m a^{-1} on April 30, 2022, and 1141 +/- 21 m a^{-1} on August 25, 2025. The south arm experienced similar trends of upglacier velocity propagation as the north arm, except that the greatest velocities occurred closest to the terminus and then decreased in magnitude to a distance approximately 20 km upglacier.

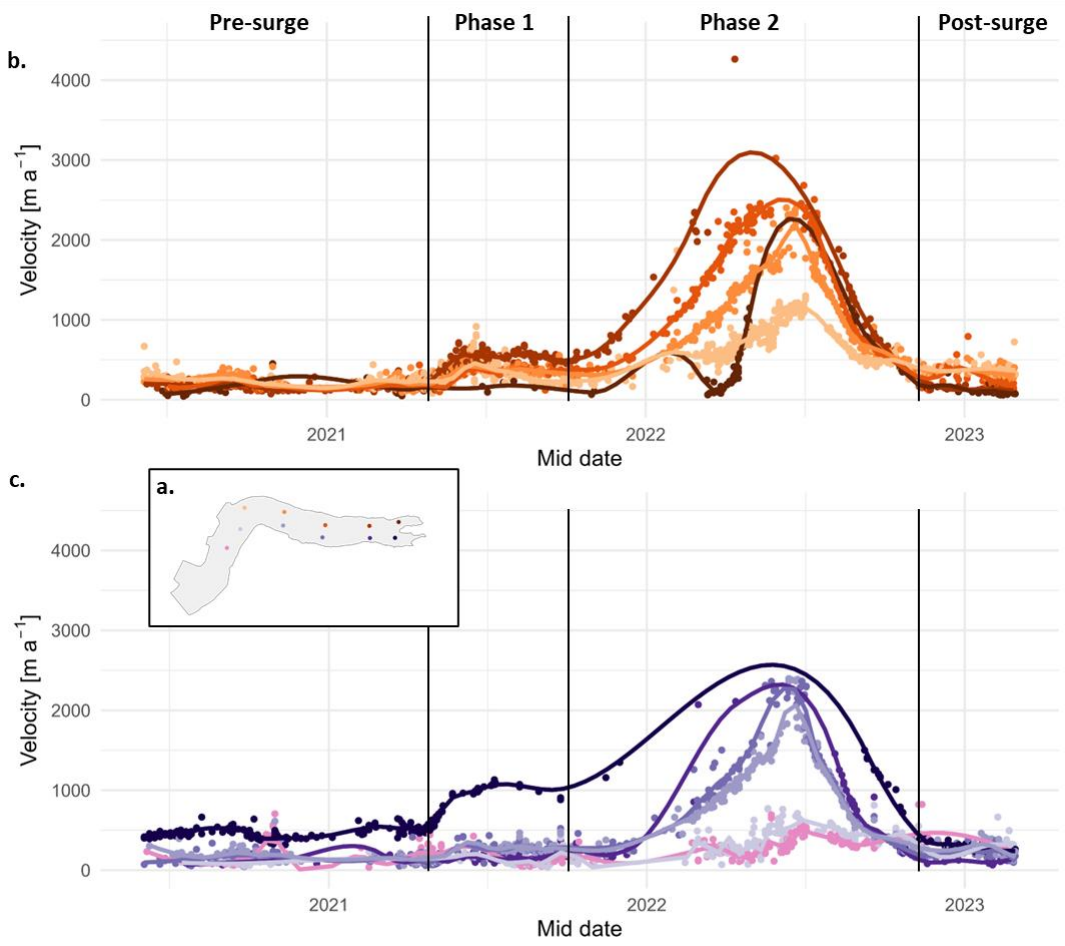

Figure 12. (a) Velocity at 11 points along the (b) north and (c) south arms at Nàłùdäy from June 2020 to February 2023, extracted from individual NASA ITS_LIVE image pair velocities with a separation of 7-45 days. Best-fit lines are based on a local polynomial regression with a degree of smoothing of 0.1. Surge phases are referred to in the Discussion.

During the surge there was an increase in velocities along the icefall connecting Dusty Glacier to Nàłùdäy, which peaked in June 2022 at 1647 +/- 62 m a^{-1} in the middle of the icefall (Fig. 13). Velocity increases in summer 2022 decreased in magnitude as they progressed from the centrepoint of the icefall into Nàłùdäy, where it enters at approximately 25 km upglacier from the terminus. Velocity increases also decreased in magnitude as they progressed from the center of the icefall towards Dusty Glacier, with the velocity changes at the top of the icefall during 2021-2022 surge barely distinguishable from those at other times.

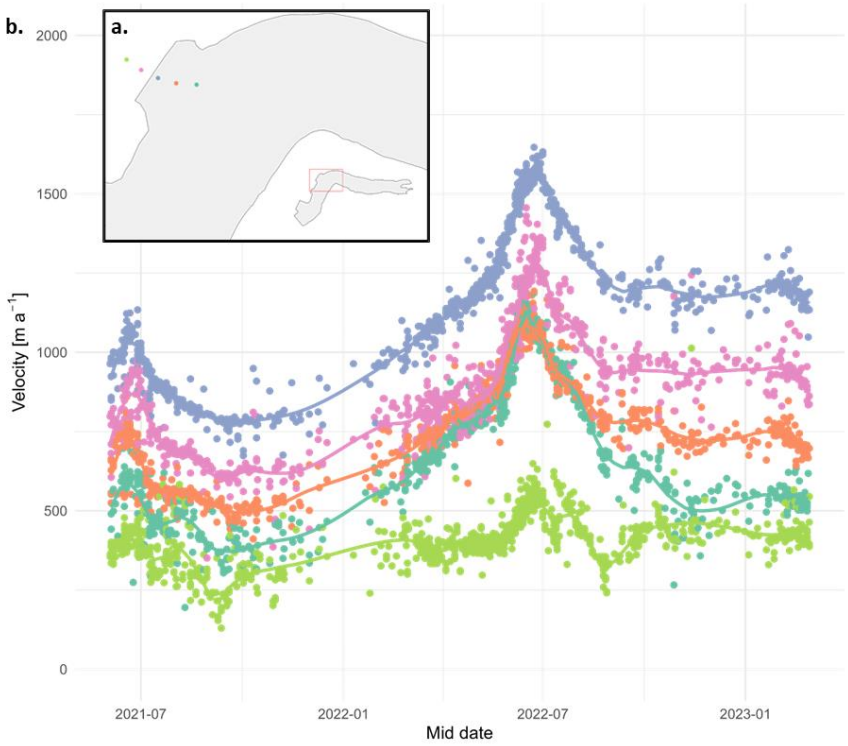

Figure 13. (a) Velocity at 5 points along the icefall between Dusty Glacier and Nàłùdäy from June 2021 to February 2023. (b) Velocities extracted from individual image pair velocities from NASA ITS_LIVE with a separation of 7-45 days. Regression is a local polynomial with a degree of smoothing of 0.1.

2.4.3.2 Longitudinal strain rates

Longitudinal strain rates can provide information about which regions of a glacier are undergoing deformation in the form of surface extension and compression at a given period of time (Cuffey & Paterson, 2010). Nàłùdäy has had consistent extension occurring across the glacier terminus, in the lowermost elevation band (500-600 m), since the 2008-2009 surge (Fig. A-4). This extension likely occurs because the glacier is lake-terminating, with little resistance to flow at the ice front.

Analysis of longitudinal strain rates during the 2021-2022 surge of Nàłùdäy shows a trend of extension to compression to extension as one moves upglacier in 2022 (Fig. 14). Starting at the terminus, extension occurred in the 500-600 m elevation band, followed by compression until 800 m a.s.l, peaking with a strain rate of -0.12 a^{-1}. Positive strain rates indicated that extension occurred from 800 m up to 1200 m a.s.l, peaking at 0.07 a^{-1} in the 1100-1200 m elevation band.

Analysis of individual strain points during 2022 indicates that most of the compression that occurred was isolated along the north arm of Nàłùdäy. In both 2021 and 2022, the majority of the

compression occurred between 600 and 800 m a.s.l along the north arm of Nàłùdäy, with some points of extension occurring along the south arm in those elevation bands (Fig. 14, right panels). The 2009-2010 surge of Nàłùdäy showed similar point strain rate evolutions (Fig. A-3), with compression in 2009 and 2010 occurring in the 600-800 m elevation bands along the north arm, while extension was occurring at those elevations along the south arm.

Both prior to surge initiation and during the surge in the 1200-1300 m elevation band, where the icefall enters Nàłùdäy, compression occurred along the north arm for 3 km downglacier from the icefall entry point. This compression is isolated to the north arm, with slight extension occurring at the same elevation along the south arm. From 2019 to 2021, after ~3 km downglacier from the icefall along the north arm, the compression present below the icefall is reduced to near zero. In contrast, during the surge in 2022 the compression below the icefall only occurred over a distance of ~2 km downglacier from its entry point, with a shift to extensional strain rates occurring further downglacier across both the north and south arms.

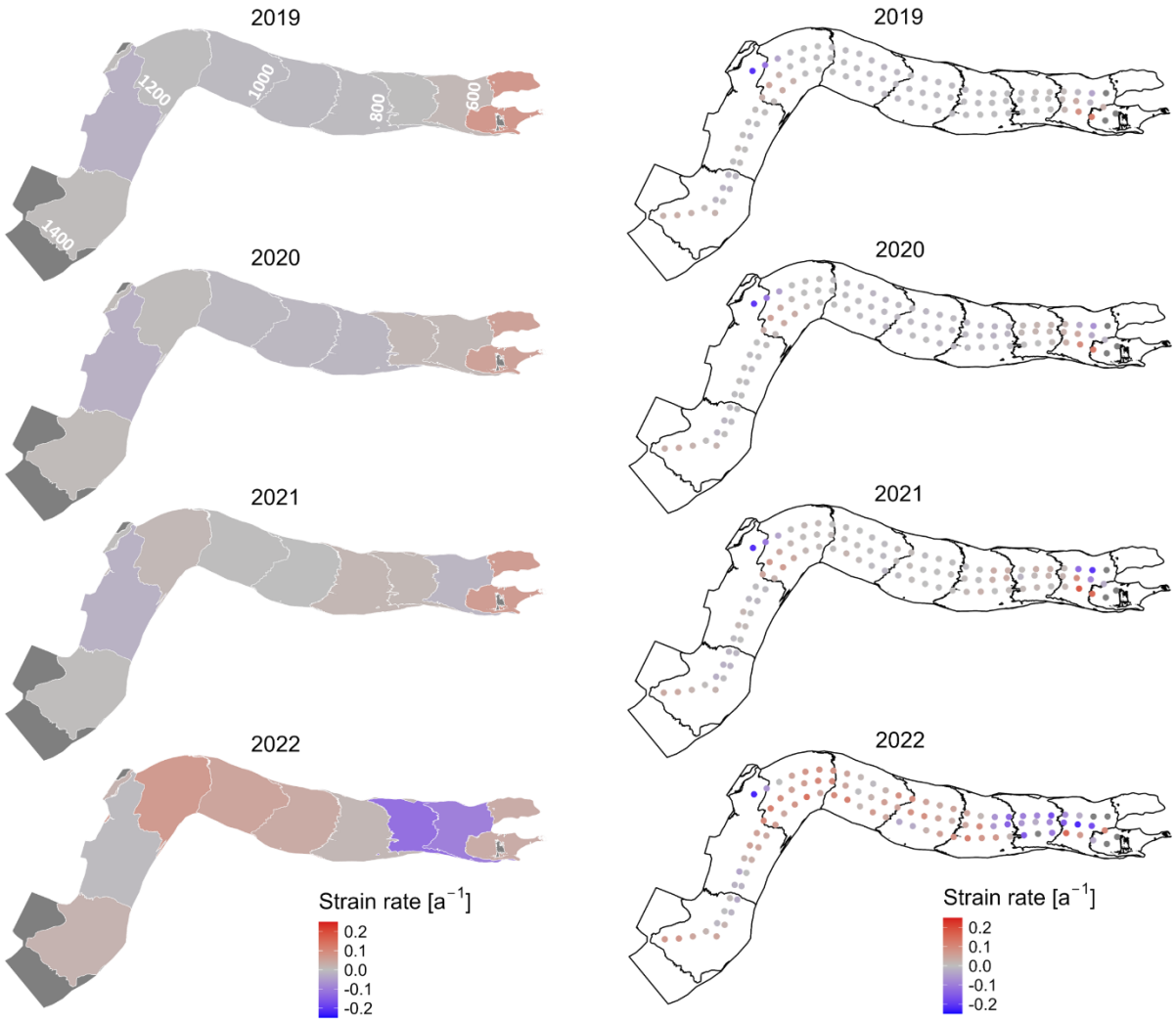

Figure 14. Annual strain rate [a^{-1}] for each elevation band and individual points calculated from annual velocity mosaics from 2019-2022 at Nàłùdäy. Positive values indicate extension; negative values indicate compression. Elevation contours are in m a.s.l.

When comparing average annual strain rates by elevation band since 1984 (Fig. A-5), a similar pattern occurred during the 2021-2022 and 2009-2010 surges (Fig. 15). This pattern is characterized by extension near the terminus, progressing to compression upglacier, then more extension above 900 m a.s.l in 2010 and 800 m a.s.l in 2022, creating a distinctive "u" shaped trend. The area of compression in the 2021-2022 surge had migrated downglacier from the area of compression in the 2009-2010 surge, and was more pronounced (Fig. 15).

During all quiescent periods (1985-1996, 1999-2008, 2011-2020) low strain rates occurred across the entire glacier (Figs. A-4, A-5). In quiescence, strain rates are generally negative, indicating

slight compression, with the exception of values for the 500-600 m elevation band, where there is relatively consistent extension.

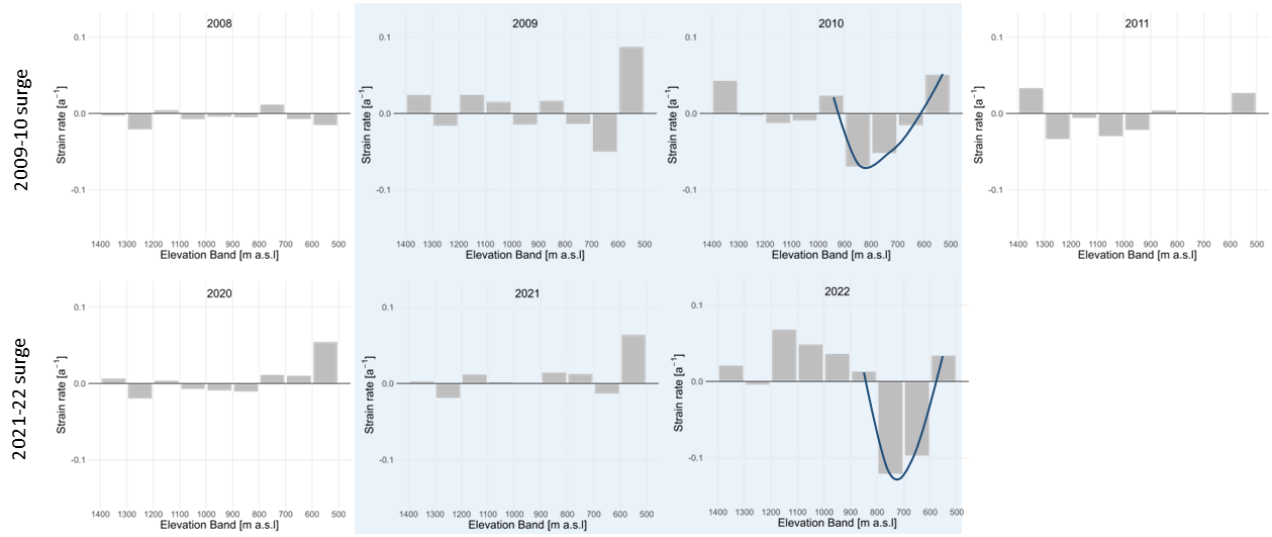

Figure 15. Average strain rates for the previous two surges of Nàłùdäy, by elevation band. Timelines are 2008-2011 and 2020-2022. Surge periods are found in the light blue box. Positive values indicate extension; negative values indicate compression.

2.5 Discussion

2.5.1 Most recent surge

The most recent surge of Nàłùdäy began in spring 2021 in a two phase initiation, after an approximately 11 year quiescent period (Bevington & Copland, 2014). This marked the 6th scientifically reported surge of Nàłùdäy (Bevington & Copland, 2014; Main, 2024), with prior historical advances being recorded by oral history of First Nations in the region, including the Champagne and Aishihik First Nations (Cruikshank, 2001) and the Tlingit First Nations (Hayman et al., 2022). The first phase of the recent surge was marked by an initial velocity increase which began approximately 3 months after a major calving from the terminus of the south arm between January 17 and 29, 2021 (Fig. A-2), with the calved ice remaining near the terminus of Nàłùdäy until early June 2021. It is difficult to know whether this calving event was one of the first expressions of the surge, or perhaps helped to trigger it. Initial velocity increases at Nàłùdäy began in May 2021, and were most pronounced at the south arm terminus and occurred in a gradual step wise fashion, with velocities along the south arm terminus rising from ~500 m a^{-1} to ~1000 m a^{-1} which plateaued from mid-June until late fall 2021 (Fig. 12). During the first phase of the surge,

velocity increases were recorded along the south arm terminus, and to a lesser extent (velocities increases up to ~600 m a^{-1}) along the north arm up to ~5 km upglacier (Fig. 12.)

The second phase of initiation began in fall 2021, when velocities first increased approximately 5 km upglacier from the terminus along the north arm. From there, acceleration propagated upglacier along the north and south arm until the icefall (~25 km upglacier), and downglacier to the south arm of the terminus first, followed by the north arm of the terminus. Upglacier propagation from January to March 2022 on Nàłùdäy has been previously reported (Van Wychen et al., 2023), but without the full context provided here. The second phase continued until peak surge velocities (4263 m a^{-1}) were recorded along the north arm at ~5 km upglacier during spring 2022. Accelerations up- and downglacier from the ~5 km north arm initiation location were delayed and at a lower magnitude. Velocities across the glacier dropped significantly by late fall 2022, and the glacier had fully returned to quiescence by end of fall 2022.

The 2021-2022 surge of Nàłùdäy displayed a unique two-arm dynamic, whereby the surge propagation transferred between the arms at various points, visible in velocity, strain rate and crevassing data. During the first phase of the surge, velocity increases occurred over the south arm terminus and upwards of ~5 km upglacier along the north arm. Crevassing in 2021 and 2022 shows a cross-arm pattern occurring near the terminus, where heavy crevassing crossed from the margins along the north arm to the terminus of the south arm, and it is only later, during winter 2023, when the north arm terminus became heavily crevassed. The downglacier propagation of surge velocities over the lowermost glacier, and the transfer between the north and south arm, is likely due to the evolving driving stress during the surge (Burgess et al., 2012). Between ~10-20 km upglacier relatively similar velocity increases occurred between the two arms. During the second surge phase, acceleration of the north arm terminus was delayed compared to that of the south arm terminus, starting only after velocities and strain rates had increased upglacier, with the south arm terminus accelerating in fall 2021 and the north arm terminus accelerating in winter 2022.

Surface elevation change of Nàłùdäy from 2019 to 2023 indicates a dynamic boundary line (DBL) for the 2021-2022 surge at approximately 875 to 900 m a.s.l. (Fig. 16). Mass transfer that occurred during the surge was mainly concentrated along the north arm, below the icefall shared with Dusty Glacier. Although the build up of the reservoir zone was present below the icefall, the acceleration of the icefall itself during the surge (Fig. 13) was likely only a result of the main trunk speeding-

up below it and not pushing from above. This is because the upper portion of Dusty Glacier above the icefall did not experience a significant acceleration during the surge, meaning that Nàłùdäy did not have an impact on the dynamics there. Below the DBL, the greatest increase in surface elevation occurred along the south arm right near the terminus, where the bulk of the ice was transferred to in the receiving zone. The DBL is also found near the transition between extensional and compressional strain rates (Fig. 14).

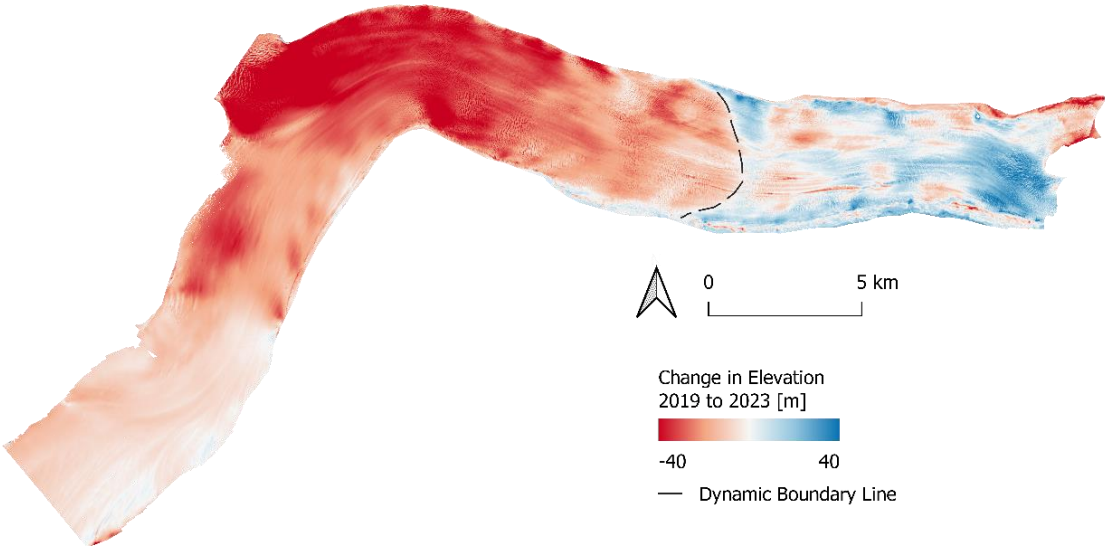

Figure 16. Elevation change map of Nàłùdäy from July 2019 to August 2023 derived from air photo SfM DEMs.

2.5.2 Evolving supraglacial hydrological networks and their link to dynamics

Supraglacial streams work to effectively transport water across the glacier surface, forming when thermal erosion from meltwater is greater than surface ablation, cauing incision (Pitcher & Smith, 2019). A marked reduction in the number of streams and moulins on the glacier surface occurred between July 2019, before the surge started, and August 2023, after the surge had stopped, even though there was an increase in individual water pixels over this period. Rather than flowing in fast-moving stream systems that are common during non-surge conditions, water was found pooling on the glacier surface during and after the surge. The increase in water pixels after the surge, but decrease in number and length of streams, indicates that post-surge water is being transported less efficiently on the glacier surface than before, often in water filled crevasses.

After surge initiation, enhanced extension (i.e., positive longitudinal strain rates; Fig. 14) due to ice acceleration below the icefall caused extensive crevassing (Fig. 9), which impacted surface topography. In turn, these new crevasses broke up the supraglacial pathways in which streams once flowed and reduced or completely stopped water flow to moulins, which then closed due to ice deformation. After the surge had terminated, and the surface pathways begin to reconnect and crevasses close, the supraglacial hydrological system reforms and eventually the same cycle will repeat itself during the next surge.

2.5.2.1 Linking hydrological inputs and surge dynamics

In summer 2019, prior to surge initiation, there was a major clustering of moulins on Nàłùdäy between 700-1000 m a.s.l, which contained 87.9% (80 moulins) of all moulins mapped that year. This region also coincided with the initiation location for the second phase of the 2021-2022 surge, as well as the peak velocity location during the surge. To understand the bed topography in this region, data is available from an AirIPR (Airborne Ice Penetrating Radar) survey that was conducted using a system slung beneath a helicopter in April 2024 (P. Wray, personal communication, August 25, 2025). The final bed map was processed to a pixel resolution of 100 m, with a median uncertainty of 11.29 m, and shows a U-shaped valley typical under glaciers caused by glacial erosion (Fig. 17; Benn & Evans, 1998).

The main moulin cluster coincides with the location of a bedrock overdeepening that occurs from ~4 to 16 km upglacier from the terminus (Fig. 18). An overdeepening describes a depression present in the bed topography beneath a glacier, where the bed slopes upwards in the direction of glacier flow (Cuffey & Paterson, 2010; Cook & Swift, 2012). In order for water to exit the overdeepening, pressure must be enough for the water to flow along this uphill slope (Cook & Swift, 2012); if insufficient pressure is available then a supercooling effect may be present, whereby water freezes to subglacial conduit walls rather than driving channel melt to keep them open (Cuffey & Paterson, 2010; Werder, 2016). The deeper the overdeepening, the greater the likelihood of disruption in connectivity of the subglacial hydrological system (Werder, 2016).

The coincident location of the moulin cluster, surge initiation location, and overdeepening, likely points to a change in drainage capacity that occurs along the front slope of the overdeepening for the surge to initiate. Bed topography, including ridges (Flowers et al., 2011) and overdeepenings (Lovell et al., 2018), have been previously highlighted as explanatory controls on glacier surging

in the study region and elsewhere. In the case of Nàłùdäy, the overdeepening may act as a reservoir, restricting flow further downglacier. Once water pressure within the overdeepening reaches a certain threshold, then water may travel over the overdeepening and promote basal sliding.

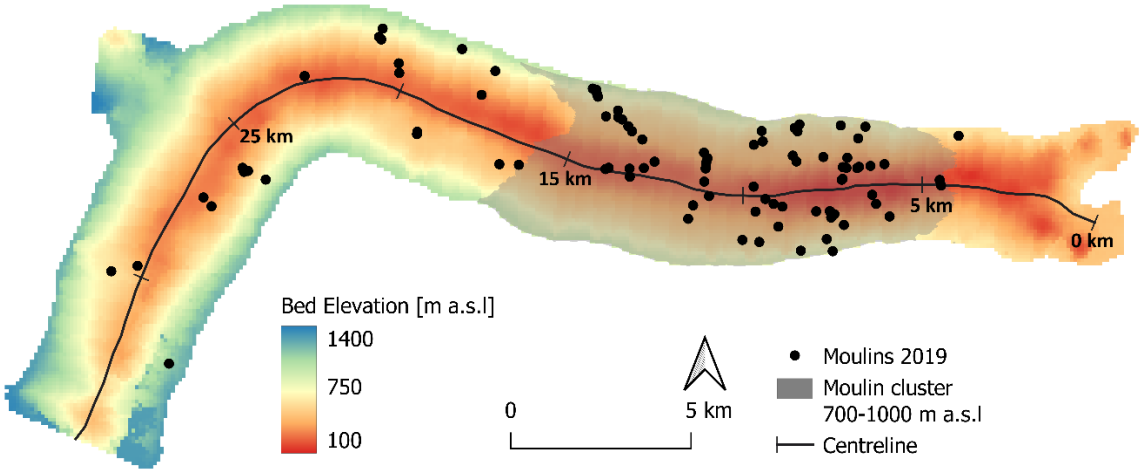

Figure 17. Bed elevation of Nàłùdäy derived from AirIPR surveys conducted in April 2024, with 2019 moulin locations marked by black dots and main moulin cluster highlighted in grey.

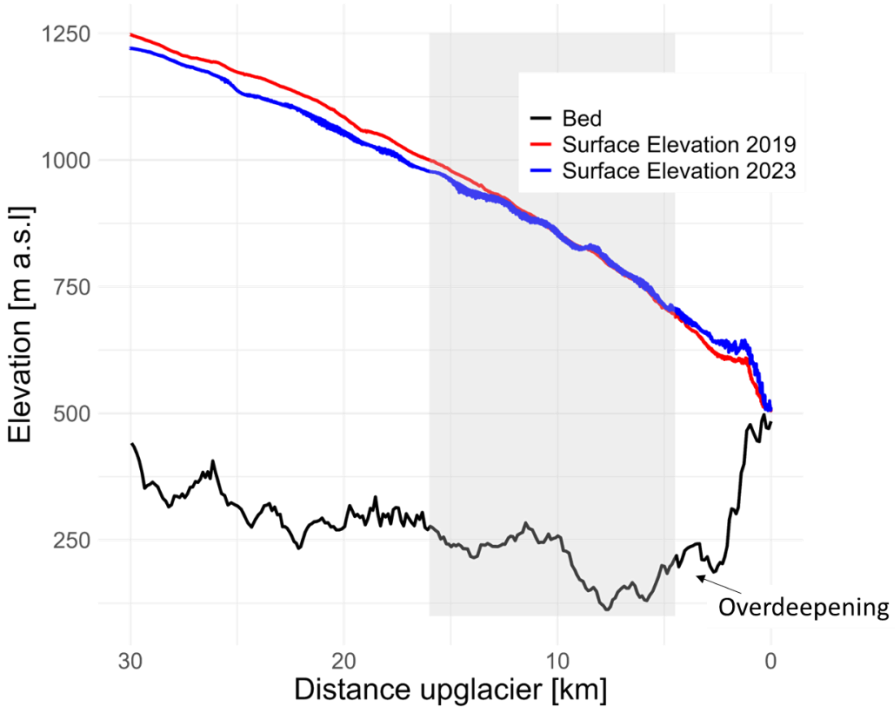

Figure 18. Bed elevation (derived from April 2024 AirIPR surveys) and surface elevations (derived from July 2019 and August 2023 air photo SfM surveys) along the centreline of Nàłùdäy, with main 2019 moulin cluster highlighted in grey.

2.5.2.2 Modelling of supraglacial hydrology

To better understand the impact of surface topography on the theoretical vs. observed location of supraglacial streams, predicted flow routing based on the 2019 and 2023 SfM DEMs was completed using ArcHydro (Fig. 19a, b; Maidment, 2008). For fast-flowing glaciers in the St. Elias Mountains, streams mapped using flow routing represent theoretical pathways rather then actual streams, as they can overestimate the amount of streams on the glacier surface (Figs. 7, 19). However, such theoretical pathways can be used to improve understanding of the role that surface topography has on stream system formation, and how changes in surface topography during a surge further impact the flow of water on the glacier surface.

The percentage of manually mapped streams which overlapped with theoretical flow pathways pre- to post-surge remained relatively similar, only changing from 59.3 to 62.9% from 2019 to 2023 (Fig. 19c, d; Table A-2). This means that although the total number and length of mapped streams decreased dramatically over this period, a similar porportion of melt was available to fill theoretical pathways. Prior to the surge in summer 2019 theoretical pathways also showed a large arborescent system, with streams connecting the entire length of the glacier surface in many long channels parallel to the glacier flow direction (Fig. 19a). In summer 2023, after the surge had terminated, theoretical DEM flow pathways indicated a less connected system, with more channels running perpendicular to glacier flow, including along previous crevasses (Fig. 19b, 20).

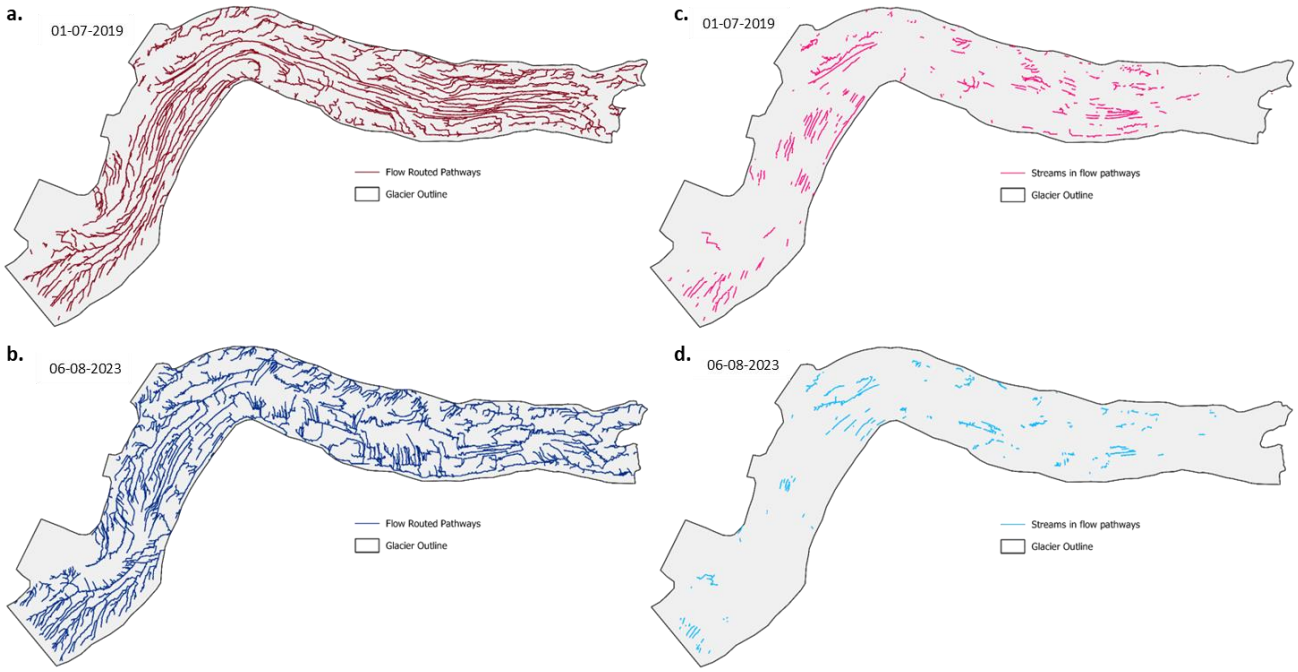

Figure 19. Theoretical flow pathways for Nàłùdäy for (a) 2019 & (b) 2023, calculated using ArcHydro Pro flow routing models on SfM Digital elevation models from summer 2019 & summer 2023, and (c, d) manually mapped streams that intersect with flow routed pathways.

During the early part of the surge extensional strain rates produced crevasses, which provide connections for supraglacial water to reach the subglacial hydrological system, enhancing the amount of melt that reaches the glacier bed (Dunse et al., 2015). As the surge progresses, and later terminates, the crevasses became water filled, enhancing pathways for water to flow across the glacier surface. This created a less efficient system of potential flow pathways as the crevasses typically occurred perpendicular to the glacier flow direction. This orientation of potential flow pathways emphasises how formation for the majority of supraglacial streams is driven by surface topography (Fig. 20).

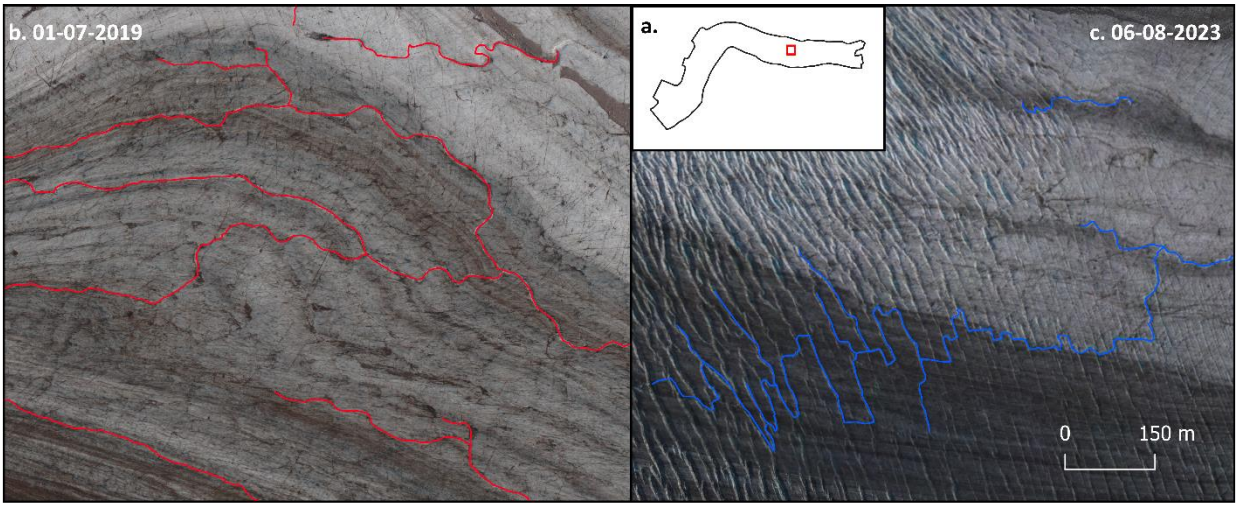

Figure 20. Mapped stream system changes at: (a) a particular location along Nàłùdäy, in (b) summer 2019 in red (pre-surge) and (c) summer 2023 in blue (post-surge), showing that after the surge crevasses are acting as supraglacial flow pathways.

Cumulative positive degree days (PDDs) from the weather station near the icefall between Nàłùdäy and Dusty Glaciers provides information about the quantity of melt occurring each year (Fig. 21). Although the greatest amount of water on the glacier surface was found in 2024 (Fig. 5), the years with the most PDDs at the date of the Sentinel-2 imagery analysed for surface water (Table 1) were 2022 and 2023. This tells us that area increases in water on the glacier surface were not due to an increase in melt, but rather due to surge-driven changes in glacier surface conditions that impacted the glacier's ability to efficiently transport water on its surface. In addition, the 2019 SfM survey was completed over a month earlier than the 2023 survey, with considerably lower PDD at the time, indicating that the decrease in streams in 2023 is not due to lower melt levels.

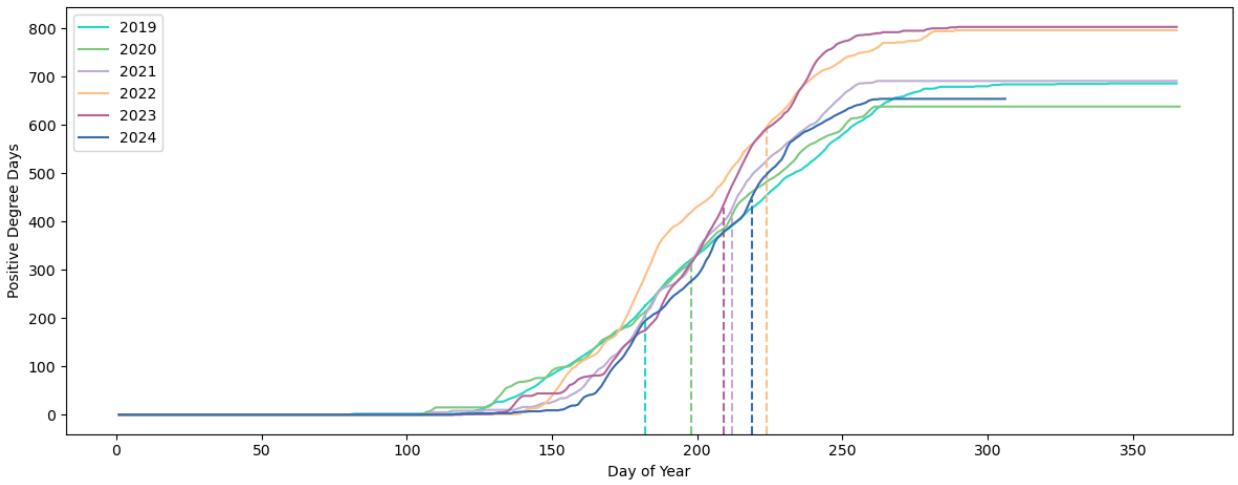

Figure 21. Cumulative positive degree days calculated for 2020 to 2024. Dashed lines represent the day of Sentinel-2 images used in section 2.4.1 (Table 1). PDD is calculated from the mean daily temperature from the Lowell Nunatak AWS for all years, except for 2019 which is based on on-glacier (60°18.458'N, 138°21.562'W) HOBO temperature data.

2.5.3 Comparison with other surges

The 2021-22 surge of Nàłùdäy is similar in duration to previous surges that have occurred there, with active phases generally lasting 1-2 years (Bevington & Copland, 2014). The length of quiescent phases between surges has been decreasing towards present day, with the first recorded quiescence (~1950-1968) at 18 years, compared to that of the two most recent quiescent phases (1998-2009, 2010-2021) at 11 years (Bevington & Copland, 2014). Previous surges were characterised by increased surface velocities, terminus advance, and heavy crevassing on the glacier surface, although lack of data has prevented a detailed assessment of their initiation location and progression. Terminus advance extents from surges since 1948-1950 have been continually decreasing, with the maximum relative area increase from quiescence to surge peak occurring during the 1983-1984 surge, with ~12 km^2 of area change (Bevington & Copland, 2014). Historical strain rates indicate a similar evolution for the 2021-2022 and 2009-2010 surges at Nàłùdäy (Fig. 15), with the 2009-2010 surge likely experiencing a similar upglacier velocity propagation as the 2021-2022 surge. Data from earlier surges is insufficient, so no direct comparisons between the 2021-2022 surge and surges prior to 2009-2010 are possible.

The 2021-2022 surge of Nàłùdäy exhibited similar characteristics to other surges that have occurred in the region, which have been used to coin the term "Alaskan-style surge", which are thought to be driven by a transition of the subglacial hydrological system from being primarily

channelized to distributed (Kamb, 1987), and/or a related change in basal till dilation (Minchew & Meyer, 2020). The most recent surge of Nàłùdäy had an active phase of approximately 1.5 years, initiating after an 11 year quiescent period, similar to that of other glaciers in the region including: Dän Zhùr (Donjek Glacier), with an active phase of ~2 years and ~12 year quiescent phase (Kochtitzky et al., 2019); Bering Glacier, with an active phase of ~2.5 to 3 years and ~13 year quiescent phase (Burgess et al., 2012); and Variegated Glacier, with an active phase of ~1 to 2 years and ~15 year quiescent phase (Eisen et al., 2005). Dusty Glacier and Fisher Glacier, also in the St Elias Mountains, have similar active phase lengths of ~2 years, with periods between surges of 32 years for Dusty (Main, 2024; Young et al., 2024) and 42 years for Fisher (Partington et al., 2025). Velocity increases at Nàłùdäy occurred in two phases, with an initial stepwise increase, followed by a drastic acceleration to the peak, similar to other surges that had distinct phases, including Bering (Burgess et al., 2012), Variegated (Eisen et al., 2005), Trapridge (Frappé & Clarke, 2007), Sit'Kusa (Nolan et al., 2021), Fisher (Partington et al., 2025) and Little Kluane (Main et al., 2024). The rapid deceleration and return to quiescence that occurred after peak velocities were observed at Nàłùdäy in summer and fall of 2022 is commonly seen in other surging glaciers in the Alaska-Yukon region (Guillet et al., 2025).

Upglacier propagation of surges has previously been seen on glaciers in Svalbard (Dunse et al., 2015; Sevestre et al., 2018), in Greenland (Müller et al., 2021), and in the Canadian High Arctic (Lauzon et al., 2023; Copland et al., 2024). For example, on Basin-3 on Austfonna Ice Cap in Svalbard, the surge initiated after the terminus destabilised (Dunse et al., 2015), similar to in the Canadian High Arctic where surges have initiated due to terminus thinning and floatation (Lauzon et al., 2023; Copland and others, 2024). Nàłùdäy is lake terminating, meaning that it could possibly experience similar terminus floatation to marine terminating glaciers, although little is known about the ice thickness or water depth at the terminus. It is therefore difficult to know if the major calving event that occurred prior to surge initiation was linked to the surge, but this should be an area for future investigation.

In the St. Elias Mountains the majority (81%) of observed glacier surges from 1985-2023 began in winter, with most others beginning in late summer/fall (Main, 2024). The timing of the most recent surge of Nàłùdäy follows both of these timelines, with the first phase of acceleration occurring in spring, and the second phase in fall. Surge termination for Nàłùdäy occurred rapidly,

beginning in summer 2022. During surge termination the velocities dropped rapidly, possibly coinciding with a subglacial water release that often occurs with the linked cavity surge mechanism (Kamb, 1987). However, due to Nàłùdäy terminating into Lake Alsek it is not possible to determine if a significant hydrological output occurred with the termination.

2.6 Summary and Conclusions

The 2021-2022 surge of Nàłùdäy is one of the few surges globally where high and medium-resolution imagery and data is available for almost the entire duration of the surge. This allows for examination of aspects of the surge not previously studied, including the connection between supraglacial hydrology and surge dynamics. Based on the findings presented here, the dynamics and hydrology of this event can be summarized as (Figs. 12, 22):

1. Pre-surge: The surge followed an 11-year quiescence period, after the 2009-2010 surge, during which annual velocities averaged 53 m a^{-1} across the lower 20 km of the glacier. The supraglacial hydrological network consisted of clusters of arborescent streams, generally terminating in moulins, draining meltwater to the subglacial hydrological system. There was a major cluster of moulins between 700-1000 m a.s.l (~5-15 km upglacier from the terminus), coinciding with a overdeepening in the basal topography. A major calving event took place in January 2021 from the south arm terminus.
2. Phase 1: The first phase of the surge comprised a step-wise increase in velocities beginning at the south arm terminus in spring 2021, and to a lesser extent along the north arm starting at ~5 km upglacier. Velocities approximately doubled, reaching ~1000 m a^{-1} near the south terminus and ~600 m a^{-1} along the north arm, and plateaued at these velocities from summer 2021 onwards. The supraglacial hydrological system was similar to that prior to surge initiation. Crevassing began to propagate upglacier starting at the south arm terminus.
3. Phase 2: The second phase initiated in fall 2021 ~5 km upglacier from the terminus along the north arm, with velocity increases propagating from this point both up- and down-glacier. Accelerations upglacier progressed across both the north and south arm until ~25 km upglacier from the terminus, past the entry of the icefall into Nàłùdäy, reducing in magnitude with distance from the initiation location. The downglacier propagation crossed to the south terminus first, which accelerated beginning in fall 2021, followed by the north arm of the terminus in spring 2022. Glacier velocities peaked in spring 2022, with the

highest recorded velocities of >4000 m a^{-1} located near the initiation location of the second phase. Crevassing progressed upglacier during the surge, initially curving from the south arm of the terminus to the north margin by winter 2022. Upglacier crevasse progression began to break the supraglacial hydrological network, causing streams to flow into crevasses. The crevasses acted as sinkpoints, connecting supraglacial streams to the subglacial system.

4. Post-surge: After the surge peak in spring 2022, velocities dropped rapidly and returned to quiescent values across the glacier by end of fall 2022. Maximum crevassing was reached post-surge in winter 2023, with the lower ~15 km of Nàłùdäy heavily crevassed. With decreased velocities, ice compression caused crevasses to start to close and water to begin to pool in them, preventing drainage to the subglacial hydrological system. Water then began to flow between crevasses, forming a new, fragmented supraglacial hydrological system of connected crevasses.

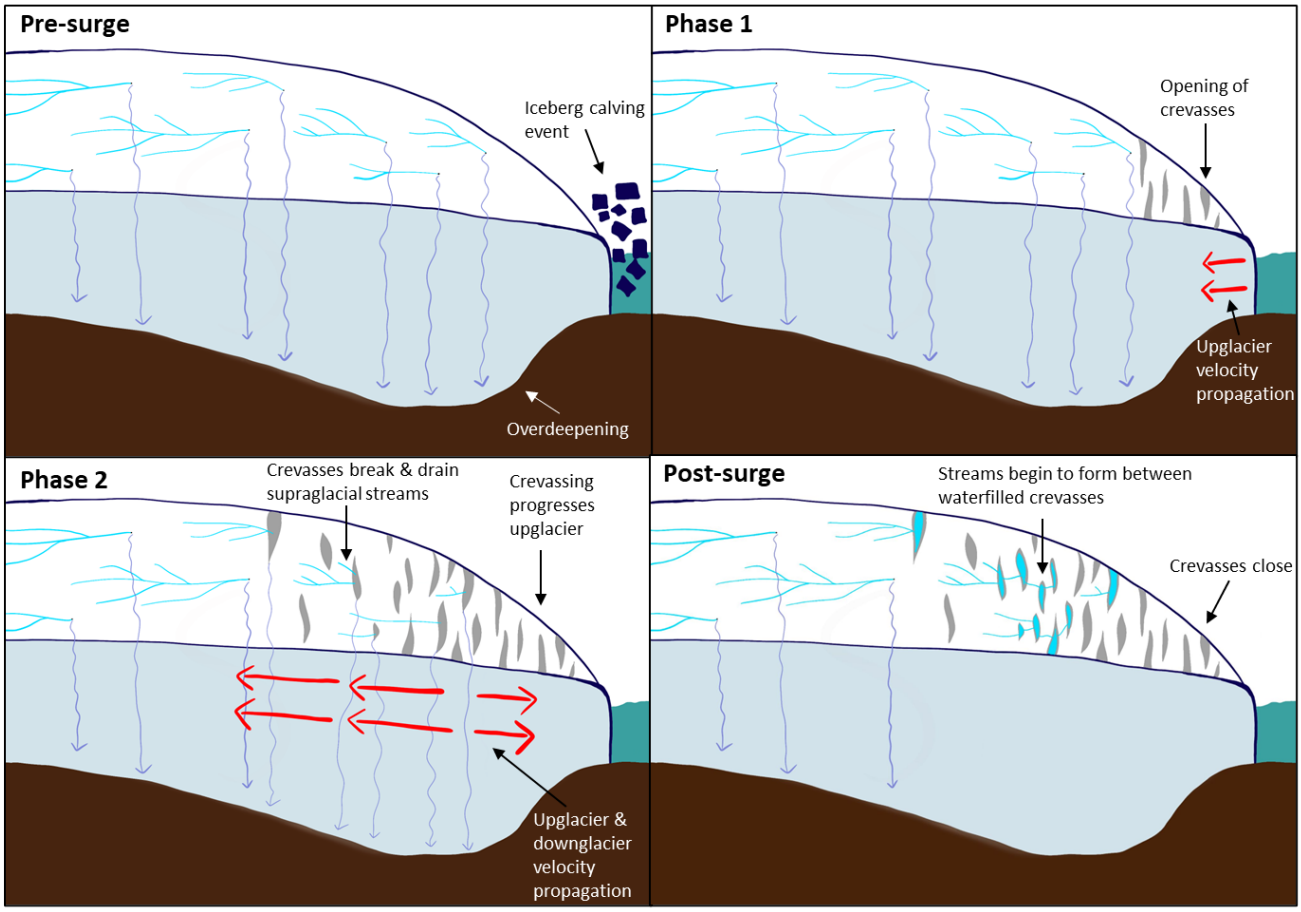

Figure 22. Schematic showing simplified phases of the 2021-2022 surge over the lower ~20 km of Nàłùdäy. Timeline of the 4 phases is presented in Fig. 12.

When analysing both glacier velocities and hydrological changes during the surge, a complex dynamic relationship is present. The spatial coincidence between the moulin clustering, surge initiation location and bed topography points to surge initiation being linked to a change in the subglacial drainage system near the overdeepening at Nàłùdäy. The forward slope in the basal depression requires significant pressure for the water to flow up it (Cuffey & Paterson, 2010), causing increased resistance during quiescence. The pre-surge location of moulin input into the basal overdeepening likely causes water to accumulate at the bed, eventually reaching the level of the overdeepening and surpassing it, which could play a significant role in surge initiation (Flowers et al., 2011). Then, as basal sliding during the surge increases, increased surface strain rate causes crevassing, which breaks up the supraglacial hydrological network and creates additional sinkpoints for meltwater to reach the glacier bed (Dunse et al., 2015). After the surge terminates

and deceleration occurs, the crevasses begin to close and become water-filled, eventually becoming potential surface flow pathways running perpendicular to glacier flow.

Timing, active phase duration and velocity characteristics of the 2021-2022 surge at Nàłùdäy, are similar to other surges that have been studied in the Alaska-Yukon region thought to be driven by subglacial changes (Kamb et al., 1985; Burgess et al., 2012; Kochtitzky et al., 2019). This surge also represents the first reported upglacier propagating surge for a lake-terminating glacier anywhere globally, a process which has been previously only seen on marine-terminating surges, where initiation has been at least partly attributed to changes in terminus floatation (Dunse et al., 2015; Lauzon et al., 2023).

Future studies at Nàłùdäy, including mapping the depth of Lake Alsek and glacier grounding line changes, will help to provide better understanding of the role of subglacial topography and floatation in driving surges of lake-terminating glaciers, and whether there are similarities to marine-terminating glacier dynamics. When possible, future surges at Nàłùdäy and elsewhere should include analysis of their changing supraglacial hydrological networks in association with their velocity changes and bed topography to determine if subglacial water storage areas, such as the overdeepening at Nàłùdäy, are important factors for surge dynamics broadly. Additionally, the application of a subglacial drainage system model to Nàłùdäy using the information about moulin clustering presented in this study will help to determine the causes and patterns of changes to the subglacial hydrological system during a surge.

Chapter 3: References

Abe, T., & Furuya, M. (2015). Winter speed-up of quiescent surge-type glaciers in Yukon, Canada. *The Cryosphere*, *9*(3), 1183–1190. https://doi.org/10.5194/tc-9-1183-2015

Alley, K. E., Scambos, T. A., Anderson, R. S., Rajaram, H., Pope, A., & Haran, T. M. (2018). Continent-wide estimates of Antarctic strain rates from Landsat 8-derived velocity grids. *Journal of Glaciology*, *64*(244), 321–332. https://doi.org/10.1017/jog.2018.23

AMAP. (2021). *Arctic Climate Change Update 2021: Key Trends and Impacts. Summary for Policy-makers.* Arctic Monitoring and Assessment Programme (AMAP).

Benn, D. I., & Evans, D. J. A. (1998). *Glaciers & glaciation*. Arnold.

Benn, D. I., Fowler, A. C., Hewitt, I., & Sevestre, H. (2019a). A general theory of glacier surges. *Journal of Glaciology*, *65*(253), 701–716. https://doi.org/10.1017/jog.2019.62

Benn, D. I., Hewitt, I. J., & Luckman, A. J. (2022). Enthalpy balance theory unifies diverse glacier surge behaviour. *Annals of Glaciology*, *63*(87–89), 88–94. https://doi.org/10.1017/aog.2023.23

Benn, D. I., Jones, R. L., Luckman, A., Fürst, J. J., Hewitt, I., & Sommer, C. (2019b). Mass and enthalpy budget evolution during the surge of a polythermal glacier: A test of theory. *Journal of Glaciology*, *65*(253), 717–731. https://doi.org/10.1017/jog.2019.63

Bevington, A., & Copland, L. (2014). Characteristics of the last five surges of Lowell Glacier, Yukon, Canada, since 1948. *Journal of Glaciology*, *60*(219), 113–123. https://doi.org/10.3189/2014JoG13J134

Bingham, R. G., Nienow, P. W., Sharp, M. J., & Copland, L. (2006). Hydrology and dynamics of a polythermal (mostly cold) High Arctic glacier. *Earth Surface Processes and Landforms*, *31*(12), 1463–1479. https://doi.org/10.1002/esp.1374

Burgess, E. W., Forster, R. R., Larsen, C. F., & Braun, M. (2012). Surge dynamics on Bering Glacier, Alaska, in 2008–2011. *The Cryosphere*, *6*(6), 1251–1262. https://doi.org/10.5194/tc-6-1251-2012

Burgess, E. W., Larsen, C. F., & Forster, R. R. (2013). Summer melt regulates winter glacier flow speeds throughout Alaska. *Geophysical Research Letters*, *40*(23), 6160–6164. https://doi.org/10.1002/2013GL058228

Chu, V. W. (2014). Greenland ice sheet hydrology: A review. *Progress in Physical Geography: Earth and Environment*, *38*(1), 19–54. https://doi.org/10.1177/0309133313507075

Chu, W., Schroeder, D. M., Seroussi, H., Creyts, T. T., Palmer, S. J., & Bell, R. E. (2016). Extensive winter subglacial water storage beneath the Greenland Ice Sheet. *Geophysical Research Letters*, *43*(24). https://doi.org/10.1002/2016GL071538

Chudley, T. R., Christoffersen, P., Doyle, S. H., Bougamont, M., Schoonman, C. M., Hubbard, B., & James, M. R. (2019). Supraglacial lake drainage at a fast-flowing Greenlandic outlet glacier. *Proceedings of the National Academy of Sciences*, *116*(51), 25468–25477. https://doi.org/10.1073/pnas.1913685116

Ciracì, E., Velicogna, I., & Swenson, S. (2020). Continuity of the Mass Loss of the World's Glaciers and Ice Caps From the GRACE and GRACE Follow-On Missions. *Geophysical Research Letters*, *47*(9), e2019GL086926. https://doi.org/10.1029/2019GL086926

Clague, J. J., & Rampton, V. N. (1982). Neoglacial Lake Alsek. *Canadian Journal of Earth Sciences*, *19*(1), 94–117. https://doi.org/10.1139/e82-008

Clarke, G. K. C. (1976). Thermal Regulation of Glacier Surging. *Journal of Glaciology*, *16*(74), 231–250. https://doi.org/10.3189/S0022143000031567

Clason, C., Mair, D. W. F., Burgess, D. O., & Nienow, P. W. (2012). Modelling the delivery of supraglacial meltwater to the ice/bed interface: Application to southwest Devon Ice Cap, Nunavut, Canada. *Journal of Glaciology*, *58*(208), 361–374. https://doi.org/10.3189/2012JoG11J129

Cogley, J. G., Hock, R., Rasmussen, L., Arendt, A., Bauder, A., Braithwaite, R., Jansson, P., Kaser, G., Möller, M., Nicholson, L., & Zemp, M. (2011). *Glossary of Glacier Mass Balance and Related Terms, IHP-VII Technical Documents in Hydrology No. 86, IACS Contribution No. 2, UNESCO-IHP, Paris.*

Cook, S. J., & Swift, D. A. (2012). Subglacial basins: Their origin and importance in glacial systems and landscapes. *Earth-Science Reviews*, *115*(4), 332–372. https://doi.org/10.1016/j.earscirev.2012.09.009

Copland, L., Hallé, D., Van Wychen, W., Lauzon, B., Dowdeswell, J. A., & Davis, J. (2024). Characteristics of the 15-year surge of Mittie Glacier, SE Ellesmere Island, Canadian Arctic. *Annals of Glaciology*, *65*, e30. https://doi.org/10.1017/aog.2024.31

Copland, L., Pope, S., Bishop, M. P., Shroder, J. F., Clendon, P., Bush, A., Kamp, U., Bae Seong, Y., & Owen, L. A. (2009). Glacier velocities across the central Karakoram. *Annals of Glaciology*, *50*(52), 41–49. https://doi.org/10.3189/172756409789624229

Copland, L., Sharp, M. J., & Nienow, P. W. (2003). Links between short-term velocity variations and the subglacial hydrology of a predominantly cold polythermal glacier. *Journal of Glaciology*, *49*(166), 337–348. https://doi.org/10.3189/172756503781830656

Cruikshank, J. (2001). Glaciers and Climate Change: Perspectives from Oral Tradition. *Arctic*, *54*(4), 377–393.

Cuffey, K. M., & Paterson, W. S. B. (2010). *The physics of glaciers* (Fourth edition). Elsevier.

Das, S. B., Joughin, I., Behn, M. D., Howat, I. M., King, M. A., Lizarralde, D., & Bhatia, M. P. (2008). Fracture Propagation to the Base of the Greenland Ice Sheet During Supraglacial Lake Drainage. *Science*, *320*(5877), 778–781. https://doi.org/10.1126/science.1153360

Dowdeswell, J. A., Hamilton, G. S., & Hagen, J. O. (1991). The duration of the active phase on surge-type glaciers: Contrasts between Svalbard and other regions. *Journal of Glaciology*, *37*(127), 388–400. https://doi.org/10.3189/S0022143000005827

Dunse, T., Schellenberger, T., Hagen, J. O., Kääb, A., Schuler, T. V., & Reijmer, C. H. (2015). Glacier-surge mechanisms promoted by a hydro-thermodynamic feedback to summer melt. *The Cryosphere*, *9*(1), 197–215. https://doi.org/10.5194/tc-9-197-2015

Eisen, O., Harrison, W. D., Raymond, C. F., Echelmeyer, K. A., Bender, G. A., & Gorda, J. L. D. (2005). Variegated Glacier, Alaska, USA: A century of surges. *Journal of Glaciology*, *51*(174), 399–406. https://doi.org/10.3189/172756505781829250

Environment and Climate Change Canada. (n.d.). *Canadian Climate Normals 1991-2020 Data* [Dataset]. https://climate.weather.gc.ca/climate_normals/results_1991_2020_e.html?searchType=stnProv&lstProvince=YT&txtCentralLatMin=0&txtCentralLatSec=0&txtCentralLongMin=0&txtCentralLongSec=0&stnID=440000000&dispBack=0

Flowers, G. E., Roux, N., Pimentel, S., & Schoof, C. G. (2011). Present dynamics and future prognosis of a slowly surging glacier. *The Cryosphere*, *5*(1), 299–313. https://doi.org/10.5194/tc-5-299-2011

Fountain, A. G., & Walder, J. S. (1998). Water flow through temperate glaciers. *Reviews of Geophysics*, *36*(3), 299–328. https://doi.org/10.1029/97RG03579

Frappé, T., & Clarke, G. K. C. (2007). Slow surge of Trapridge Glacier, Yukon Territory, Canada. *Journal of Geophysical Research: Earth Surface*, *112*(F3), 2006JF000607. https://doi.org/10.1029/2006JF000607

Gardner, A., Fahnestock, M., & Scambos, T. (2025). *MEASURES ITS_LIVE Regional Glacier and Ice Sheet Surface Velocities, Version 1. Data archived at National Snow and Ice Data Center;* [Dataset]. [object Object]. https://doi.org/10.5067/6II6VW8LLWJ7

Gleason, C. J., Smith, L. C., Chu, V. W., Legleiter, C. J., Pitcher, L. H., Overstreet, B. T., Rennermalm, A. K., Forster, R. R., & Yang, K. (2016). Characterizing supraglacial meltwater channel hydraulics on the Greenland Ice Sheet from *in situ* observations. *Earth Surface Processes and Landforms*, *41*(14), 2111–2122. https://doi.org/10.1002/esp.3977

Guillet, G., Benn, D. I., King, O., Shean, D., Schytt Mannerfelt, E., & Hugonnet, R. (2025). Global detection of glacier surges from surface velocities, elevation change and SAR backscatter data between 2000 and 2024: A test of surge mechanism theories. *Journal of Glaciology*, *71*, e88. https://doi.org/10.1017/jog.2025.10065

Hart, J. K., Young, D. S., Baurley, N. R., Robson, B. A., & Martinez, K. (2022). The seasonal evolution of subglacial drainage pathways beneath a soft-bedded glacier. *Communications Earth & Environment*, *3*(1), 152. https://doi.org/10.1038/s43247-022-00484-9

Hayman, E., James, C., & Wedge, M. (2022). Future Rivers of the Anthropocene. *Open Rivers: Rethinking Water, Place & Community*. https://doi.org/10.24926/2471190X.8306

Hill, T., & Dow, C. F. (2021). Modeling the Dynamics of Supraglacial Rivers and Distributed Meltwater Flow With the Subaerial Drainage System (SaDS) Model. *Journal of Geophysical Research: Earth Surface*, *126*(12), e2021JF006309. https://doi.org/10.1029/2021JF006309

Holmlund, P. (1988). Internal Geometry and Evolution of Moulins, Storglaciären, Sweden. *Journal of Glaciology*, *34*(117), 242–248. https://doi.org/10.3189/S0022143000032305

Irvine-Fynn, T. D. L., Hodson, A. J., Moorman, B. J., Vatne, G., & Hubbard, A. L. (2011). Polythermal Glacier Hydrology: A Review. *Reviews of Geophysics*, *49*(4), 2010RG000350. https://doi.org/10.1029/2010RG000350

Jiskoot, H. (2011). Glacier Surging. In *Encyclopedia of snow, ice and glaciers* (pp. 415–427). Springer.

Kääb, A., Bazilova, V., Leclercq, P. W., Mannerfelt, E. S., & Strozzi, T. (2023). Global clustering of recent glacier surges from radar backscatter data, 2017–2022. *Journal of Glaciology*, *69*(277), 1515–1523. https://doi.org/10.1017/jog.2023.35

Kamb, B. (1987). Glacier surge mechanism based on linked cavity configuration of the basal water conduit system. *Journal of Geophysical Research: Solid Earth*, *92*(B9), 9083–9100. https://doi.org/10.1029/JB092iB09p09083

Kamb, B., Raymond, C. F., Harrison, W. D., Engelhardt, H., Echelmeyer, K. A., Humphrey, N., Brugman, M. M., & Pfeffer, T. (1985). Glacier Surge Mechanism: 1982-1983 Surge of Variegated Glacier, Alaska. *Science*, *227*(4686), 469–479. https://doi.org/10.1126/science.227.4686.469

Karlstrom, L., & Yang, K. (2016). Fluvial supraglacial landscape evolution on the Greenland Ice Sheet. *Geophysical Research Letters*, *43*(6), 2683–2692. https://doi.org/10.1002/2016GL067697

King, L., Hassan, M., Yang, K., & Flowers, G. (2016). Flow Routing for Delineating Supraglacial Meltwater Channel Networks. *Remote Sensing*, *8*(12), 988. https://doi.org/10.3390/rs8120988

Knighton, A. (1981). Channel form and Flow Characteristics of Supraglacial Streams, Austre Okstindbreen, Norway. *Arctic and Alpine Research*, *13*(3), 295–306. https://doi.org/10.1080/00040851.1981.12004250

Kochtitzky, W., Jiskoot, H., Copland, L., Enderlin, E., Mcnabb, R., Kreutz, K., & Main, B. (2019). Terminus advance, kinematics and mass redistribution during eight surges of Donjek Glacier, St. Elias Range, Canada, 1935 to 2016. *Journal of Glaciology*, *65*(252), 565–579. https://doi.org/10.1017/jog.2019.34

Lampkin, D. J., & VanderBerg, J. (2011). A preliminary investigation of the influence of basal and surface topography on supraglacial lake distribution near Jakobshavn Isbrae, western Greenland. *Hydrological Processes*, *25*(21), 3347–3355. https://doi.org/10.1002/hyp.8170

Lauzon, B., Copland, L., Van Wychen, W., Kochtitzky, W., McNabb, R., & Dahl-Jensen, D. (2023). Dynamics throughout a complete surge of Iceberg Glacier on western Axel Heiberg Island, Canadian High Arctic. *Journal of Glaciology*, *69*(277), 1333–1350. https://doi.org/10.1017/jog.2023.20

Leclercq, P. W., Kääb, A., & Altena, B. (2021). Brief communication: Detection of glacier surge activity using cloud computing of Sentinel-1 radar data. *The Cryosphere*, *15*(10), 4901–4907. https://doi.org/10.5194/tc-15-4901-2021

Lovell, A. M., Carr, J. R., & Stokes, C. R. (2018). Topographic controls on the surging behaviour of Sabche Glacier, Nepal (1967 to 2017). *Remote Sensing of Environment*, *210*, 434–443. https://doi.org/10.1016/j.rse.2018.03.036

Lu, Y., Yang, K., Lu, X., Smith, L. C., Sole, A. J., Livingstone, S. J., Fettweis, X., & Li, M. (2020). Diverse supraglacial drainage patterns on the Devon ice Cap, Arctic Canada. *Journal of Maps*, *16*(2), 834–846. https://doi.org/10.1080/17445647.2020.1838353

Maidment, D. R. (Ed.). (2008). *Arc hydro: GIS for water resources* (1. ed., [Nachdr.]). ESRI Press.

Main, B. (2024). *Glacier velocities and ice dynamics in the St. Elias Mountains, Yukon-Alaska* [University of Ottawa]. http://dx.doi.org/10.20381/ruor-30030

Main, B., Copland, L., Flowers, G. E., Dow, C. F., Van Wychen, W., Samsonov, S., & Kochtitzky, W. (2024). Topographic and hydrological controls on partial and full surges of Little Kluane Glacier, Yukon. *Journal of Glaciology*, *70*, e42. https://doi.org/10.1017/jog.2024.35

Maussion, F., Hock, R., Paul, F., Raup, B., Rastner, P., Zemp, M., Andreassen, L., Barr, I., Bolch, T., Kochtitzky, W., McNabb, R., & Tielidze, L. (2023). *The Randolph Glacier Inventory version 7.0 User guide*. https://doi.org/10.5281/ZENODO.8362857

McFeeters, S. K. (1996). The use of the Normalized Difference Water Index (NDWI) in the delineation of open water features. *International Journal of Remote Sensing*, *17*(7), 1425–1432. https://doi.org/10.1080/01431169608948714

Medrzycka, D. (2022). *Contrasting Glacier Behaviour, and Methods for Monitoring Glacier Change, in the Northern Canadian Arctic Archipelago* [Université d'Ottawa / University of Ottawa]. http://ruor.uottawa.ca/handle/10393/43981

Medrzycka, D., Copland, L., Thomson, L., Kochtitzky, W., & Smeda, B. (2025). Review of methodological considerations and recommendations for mapping remote glaciers from aerial photography surveys in suboptimal conditions. *Geoscientific Instrumentation, Methods and Data Systems*, *14*(1), 69–90. https://doi.org/10.5194/gi-14-69-2025

Meier, M. F., & Post, A. (1969). What are glacier surges? *Canadian Journal of Earth Sciences*, *6*(4), 807–817. https://doi.org/10.1139/e69-081

Minchew, B. M., & Meyer, C. R. (2020). Dilation of subglacial sediment governs incipient surge motion in glaciers with deformable beds. *Proceedings of the Royal Society A: Mathematical, Physical and Engineering Sciences*, *476*(2238), 20200033. https://doi.org/10.1098/rspa.2020.0033

Mountain Research Initiative EDW Working Group. (2015). Elevation-dependent warming in mountain regions of the world. *Nature Climate Change*, *5*(5), 424–430. https://doi.org/10.1038/nclimate2563

Müller, L., Horwath, M., Scheinert, M., Mayer, C., Ebermann, B., Floricioiu, D., Krieger, L., Rosenau, R., & Vijay, S. (2021). Surges of Harald Moltke Bræ, north-western Greenland: Seasonal modulation and initiation at the terminus. *The Cryosphere*, *15*(7), 3355–3375. https://doi.org/10.5194/tc-15-3355-2021

Murray, T., Strozzi, T., Luckman, A., Jiskoot, H., & Christakos, P. (2003). Is there a single surge mechanism? Contrasts in dynamics between glacier surges in Svalbard and other regions. *Journal of Geophysical Research: Solid Earth*, *108*(B5), 2002JB001906. https://doi.org/10.1029/2002JB001906

Nolan, A., Kochtitzky, W., Enderlin, E. M., McNabb, R., & Kreutz, K. J. (2021). Kinematics of the exceptionally-short surge cycles of Sít' Kusá (Turner Glacier), Alaska, from 1983 to 2013. *Journal of Glaciology*, *67*(264), 744–758. https://doi.org/10.1017/jog.2021.29

Nye, J. F. (1965). The Flow of a Glacier in a Channel of Rectangular, Elliptic or Parabolic Cross-Section. *Journal of Glaciology*, *5*(41), 661–690. https://doi.org/10.3189/S0022143000018670

Partington, G. (2023). *Reconstructing the Surge History and Dynamics of Fisher Glacier, Yukon, 1948-2022* [University of Ottawa]. http://dx.doi.org/10.20381/ruor-29290

Partington, G., Copland, L., Lauzon, B., Medrzycka, D., Main, B., Kochtitzky, W., & Dow, C. (2025). Surge history and dynamics of Fisher Glacier, Yukon, 1948-2022. *Journal of Glaciology*, 1–41. https://doi.org/10.1017/jog.2025.10084

Pitcher, L. H., & Smith, L. C. (2019). Supraglacial Streams and Rivers. *Annual Review of Earth and Planetary Sciences*, *47*(1), 421–452. https://doi.org/10.1146/annurev-earth-053018-060212

Post, A. (1969). Distribution of Surging Glaciers in Western North America. *Journal of Glaciology*, *8*(53), 229–240. https://doi.org/10.3189/S0022143000031221

Rawlins, L. D., Rippin, D. M., Sole, A. J., Livingstone, S. J., & Yang, K. (2023). Seasonal evolution of the supraglacial drainage network at Humboldt Glacier, northern Greenland, between 2016 and 2020. *The Cryosphere*, *17*(11), 4729–4750. https://doi.org/10.5194/tc-17-4729-2023

RGI Consortium. (2023). *Randolph Glacier Inventory—A Dataset of Global Glacier Outlines, Version 7.0* [Dataset]. NASA National Snow and Ice Data Center Distributed Active Archive Center. https://doi.org/10.5067/F6JMOVY5NAVZ

Robin, G. D. Q. (1955). Ice Movement and Temperature Distribution in Glaciers and Ice Sheets. *Journal of Glaciology*, *2*(18), 523–532. https://doi.org/10.3189/002214355793702028

Röthlisberger, H. (1972). Water Pressure in Intra- and Subglacial Channels. *Journal of Glaciology*, *11*(62), 177–203. https://doi.org/10.3189/S0022143000022188

Rounce, D. R., Hock, R., Maussion, F., Hugonnet, R., Kochtitzky, W., Huss, M., Berthier, E., Brinkerhoff, D., Compagno, L., Copland, L., Farinotti, D., Menounos, B., & McNabb, R. W. (2023). Global glacier change in the 21st century: Every increase in temperature matters. *Science*, *379*(6627), 78–83. https://doi.org/10.1126/science.abo1324

Schoof, C. (2010). Ice-sheet acceleration driven by melt supply variability. *Nature*, *468*(7325), 803–806. https://doi.org/10.1038/nature09618

Sevestre, H., & Benn, D. I. (2015). Climatic and geometric controls on the global distribution of surge-type glaciers: Implications for a unifying model of surging. *Journal of Glaciology*, *61*(228), 646–662. https://doi.org/10.3189/2015JoG14J136

Sevestre, H., Benn, D. I., Luckman, A., Nuth, C., Kohler, J., Lindbäck, K., & Pettersson, R. (2018). Tidewater Glacier Surges Initiated at the Terminus. *Journal of Geophysical Research: Earth Surface*, *123*(5), 1035–1051. https://doi.org/10.1029/2017JF004358

Smith, L. C., Andrews, L. C., Pitcher, L. H., Overstreet, B. T., Rennermalm, Å. K., Cooper, M. G., Cooley, S. W., Ryan, J. C., Miège, C., Kershner, C., & Simpson, C. E. (2021). Supraglacial River Forcing of Subglacial Water Storage and Diurnal Ice Sheet Motion. *Geophysical Research Letters*, *48*(7), e2020GL091418. https://doi.org/10.1029/2020GL091418

Smith, L. C., Chu, V. W., Yang, K., Gleason, C. J., Pitcher, L. H., Rennermalm, A. K., Legleiter, C. J., Behar, A. E., Overstreet, B. T., Moustafa, S. E., Tedesco, M., Forster, R. R., LeWinter, A. L., Finnegan, D. C., Sheng, Y., & Balog, J. (2015). Efficient meltwater drainage through supraglacial streams and rivers on the southwest Greenland ice sheet. *Proceedings of the National Academy of Sciences*, *112*(4), 1001–1006. https://doi.org/10.1073/pnas.1413024112

St Germain, S. L., & Moorman, B. J. (2019). Long-term observations of supraglacial streams on an Arctic glacier. *Journal of Glaciology*, *65*(254), 900–911. https://doi.org/10.1017/jog.2019.60

Taylor, P. C., Boeke, R. C., Boisvert, L. N., Feldl, N., Henry, M., Huang, Y., Langen, P. L., Liu, W., Pithan, F., Sejas, S. A., & Tan, I. (2022). Process Drivers, Inter-Model Spread, and the Path Forward: A Review of Amplified Arctic Warming. *Frontiers in Earth Science*, *9*, 758361. https://doi.org/10.3389/feart.2021.758361

Thomson, L. I., & Copland, L. (2017). Multi-decadal reduction in glacier velocities and mechanisms driving deceleration at polythermal White Glacier, Arctic Canada. *Journal of Glaciology*, *63*(239), 450–463. https://doi.org/10.1017/jog.2017.3

Togaibekov, A., Gimbert, F., Gilbert, A., & Walpersdorf, A. (2024). Observing and Modeling Short-Term Changes in Basal Friction During Rain-Induced Speed-Ups on an Alpine Glacier. *Geophysical Research Letters*, *51*(14), e2023GL107999. https://doi.org/10.1029/2023GL107999

UNESCO. (n.d.). *World Heritage List: Kluane / Wrangell-St. Elias / Glacier Bay / Tatshenshini-Alsek*. https://web.archive.org/web/20170129025343/http://whc.unesco.org/en/list/72/

Van Wychen, W., Bayer, C., Copland, L., Brummell, E., & Dow, C. (2023). Radarsat Constellation Mission Derived Winter Glacier Velocities for the St. Elias Icefield, Yukon/Alaska: 2022 and 2023. *Canadian Journal of Remote Sensing*, *49*(1), 2264395. https://doi.org/10.1080/07038992.2023.2264395

Van Wychen, W., Jiskoot, H., Shannon, K., & Gorwill, C. (2025). The long multiphase trunk–tributary surge history of the high-Arctic Chapman Glacier, 1959–2023. *Arctic, Antarctic, and Alpine Research*, *57*(1), 2441541. https://doi.org/10.1080/15230430.2024.2441541

Werder, M. A. (2016). The hydrology of subglacial overdeepenings: A new supercooling threshold formula. *Geophysical Research Letters*, *43*(5), 2045–2052. https://doi.org/10.1002/2015gl067542

Williamson, S. N., Zdanowicz, C., Anslow, F. S., Clarke, G. K. C., Copland, L., Danby, R. K., Flowers, G. E., Holdsworth, G., Jarosch, A. H., & Hik, D. S. (2020). Evidence for Elevation-Dependent Warming in the St. Elias Mountains, Yukon, Canada. *Journal of Climate*, *33*(8), 3253–3269. https://doi.org/10.1175/JCLI-D-19-0405.1

Willis, I. C. (1995). Intra-annual variations in glacier motion: A review. *Progress in Physical Geography: Earth and Environment*, *19*(1), 61–106. https://doi.org/10.1177/030913339501900104

Wyatt, F. R., & Sharp, M. J. (2015). Linking surface hydrology to flow regimes and patterns of velocity variability on Devon Ice Cap, Nunavut. *Journal of Glaciology*, *61*(226), 387–399. https://doi.org/10.3189/2015JoG14J109

Xu, S., Chen, M., Feng, T., Zhan, L., Zhou, L., & Yu, G. (2021). Use ggbreak to Effectively Utilize Plotting Space to Deal With Large Datasets and Outliers. *Frontiers in Genetics*, *12*, 774846. https://doi.org/10.3389/fgene.2021.774846

Yang, K., & Smith, L. C. (2012). Supraglacial Streams on the Greenland Ice Sheet Delineated From Combined Spectral–Shape Information in High-Resolution Satellite Imagery. *IEEE Geoscience and Remote Sensing Letters*, *10*(4), 801–805. https://doi.org/10.1109/LGRS.2012.2224316

Yang, K., Smith, L. C., Sole, A., Livingstone, S. J., Cheng, X., Chen, Z., & Li, M. (2019). Supraglacial rivers on the northwest Greenland Ice Sheet, Devon Ice Cap, and Barnes Ice Cap mapped using Sentinel-2 imagery. *International Journal of Applied Earth Observation and Geoinformation*, *78*, 1–13. https://doi.org/10.1016/j.jag.2019.01.008

Young, E. M., Flowers, G. E., Jiskoot, H., & Gibson, H. D. (2024). Reconstructing Glacier Surge Kinematics Using a Numerical Ice-Flow Model Applied to the Dusty Glacier, St. Elias Mountains, Canada. *Geophysical Research Letters*, *51*(10), e2023GL107386. https://doi.org/10.1029/2023GL107386

Zemp, M., Huss, M., Thibert, E., Eckert, N., McNabb, R., Huber, J., Barandun, M., Machguth, H., Nussbaumer, S. U., Gärtner-Roer, I., Thomson, L., Paul, F., Maussion, F., Kutuzov, S., & Cogley, J. G. (2019). Global glacier mass changes and their contributions to sea-level rise from 1961 to 2016. *Nature*, *568*(7752), 382–386. https://doi.org/10.1038/s41586-019-1071-0

Zwally, H. J., Abdalati, W., Herring, T., Larson, K., Saba, J., & Steffen, K. (2002). Surface Melt-Induced Acceleration of Greenland Ice-Sheet Flow. *Science*, *297*(5579), 218–222. https://doi.org/10.1126/science.1072708

Chapter 4: Appendices

Table A-1. Sentinel-1 images used in the creation of annual winter maximum images for backscatter analysis using Google Earth Engine.

Year	Number of ascending images	Image IDs
2020	18	S1A_IW_GRDH_1SDV_20200204T025456_20200204T025521_031097_0392CA_1FBA S1A_IW_GRDH_1SDV_20200216T025456_20200216T025521_031272_0398D4_6D9D S1A_IW_GRDH_1SDV_20200228T025455_20200228T025520_031447_039ED5_41B7 S1A_IW_GRDH_1SDV_20200311T025456_20200311T025521_031622_03A4E8_0775 S1A_IW_GRDH_1SDV_20200323T025456_20200323T025521_031797_03AB14_3E46 S1A_IW_GRDH_1SDV_20200404T025456_20200404T025521_031972_03B13B_375F S1A_IW_GRDH_1SDV_20200416T025457_20200416T025522_032147_03B762_391E S1A_IW_GRDH_1SDV_20200428T025457_20200428T025522_032322_03BD86_F2A8 S1B_IW_GRDH_1SDV_20200110T030222_20200110T030251_019749_025569_A6D4 S1B_IW_GRDH_1SDV_20200122T030222_20200122T030251_019924_025AFD_29C1 S1B_IW_GRDH_1SDV_20200203T030222_20200203T030251_020099_0260A5_B46F S1B_IW_GRDH_1SDV_20200215T030221_20200215T030250_020274_026646_FAF1 S1B_IW_GRDH_1SDV_20200227T030221_20200227T030250_020449_026BE8_3A76 S1B_IW_GRDH_1SDV_20200310T030221_20200310T030250_020624_027177_4122 S1B_IW_GRDH_1SDV_20200322T030221_20200322T030250_020799_027701_EF71 S1B_IW_GRDH_1SDV_20200403T030222_20200403T030251_020974_027C88_8A49 S1B_IW_GRDH_1SDV_20200415T030222_20200415T030251_021149_028212_EB20 S1B_IW_GRDH_1SDV_20200427T030223_20200427T030252_021324_028798_57A5
2021	19	S1A_IW_GRDH_1SDV_20210105T025503_20210105T025528_035997_04378D_74E2 S1A_IW_GRDH_1SDV_20210129T025502_20210129T025527_036347_0443CE_9D54 S1A_IW_GRDH_1SDV_20210210T025502_20210210T025527_036522_0449E2_05B4 S1A_IW_GRDH_1SDV_20210222T025502_20210222T025527_036697_045000_315C S1A_IW_GRDH_1SDV_20210306T025501_20210306T025526_036872_04560D_23AC S1A_IW_GRDH_1SDV_20210318T025501_20210318T025526_037047_045C2C_C021 S1A_IW_GRDH_1SDV_20210330T025502_20210330T025527_037222_046238_8C91 S1A_IW_GRDH_1SDV_20210411T025502_20210411T025527_037397_046840_6D42 S1A_IW_GRDH_1SDV_20210423T025503_20210423T025528_037572_046E50_5764 S1B_IW_GRDH_1SDV_20210104T030229_20210104T030258_024999_02F9A6_E148 S1B_IW_GRDH_1SDV_20210116T030228_20210116T030257_025174_02FF4B_33B2 S1B_IW_GRDH_1SDV_20210128T030228_20210128T030257_025349_0304D6_D003 S1B_IW_GRDH_1SDV_20210209T030227_20210209T030256_025524_030A8D_79E4 S1B_IW_GRDH_1SDV_20210221T030227_20210221T030256_025699_03103C_9ED5 S1B_IW_GRDH_1SDV_20210305T030227_20210305T030256_025874_0315F9_C37D S1B_IW_GRDH_1SDV_20210317T030227_20210317T030256_026049_031BA4_7658 S1B_IW_GRDH_1SDV_20210329T030227_20210329T030256_026224_03212B_FCE0 S1B_IW_GRDH_1SDV_20210410T030228_20210410T030257_026399_0326BA_D21C S1B_IW_GRDH_1SDV_20210422T030228_20210422T030257_026574_032C57_A9BE
2022	7	S1A_IW_GRDH_1SDV_20220124T025508_20220124T025533_041597_04F29F_791F S1A_IW_GRDH_1SDV_20220205T025507_20220205T025532_041772_04F89A_AE6E S1A_IW_GRDH_1SDV_20220217T025507_20220217T025532_041947_04FEB8_66EB S1A_IW_GRDH_1SDV_20220301T025507_20220301T025532_042122_0504B5_85BF S1A_IW_GRDH_1SDV_20220313T025507_20220313T025532_042297_050AA8_5E7C S1A_IW_GRDH_1SDV_20220406T025508_20220406T025533_042647_051688_5569 S1A_IW_GRDH_1SDV_20220418T025508_20220418T025533_042822_051C69_3902
2023	3	S1A_IW_GRDH_1SDV_20230212T025513_20230212T025538_047197_05A9B2_BAD3 S1A_IW_GRDH_1SDV_20230320T025513_20230320T025538_047722_05BB7C_890D S1A_IW_GRDH_1SDV_20230401T025513_20230401T025538_047897_05C158_8D7E
2024	5	S1A_IW_GRDH_1SDV_20240102T025519_20240102T025544_051922_0645E8_6795 S1A_IW_GRDH_1SDV_20240126T025519_20240126T025544_052272_0651BE_C938 S1A_IW_GRDH_1SDV_20240326T025518_20240326T025543_053147_067043_0E31 S1A_IW_GRDH_1SDV_20240407T025519_20240407T025544_053322_0676F1_57A1 S1A_IW_GRDH_1SDV_20240419T025519_20240419T025544_053497_067DE6_5D39

Figure A-1. Collapse features identified on 2019 SfM air photo orthomosaic.

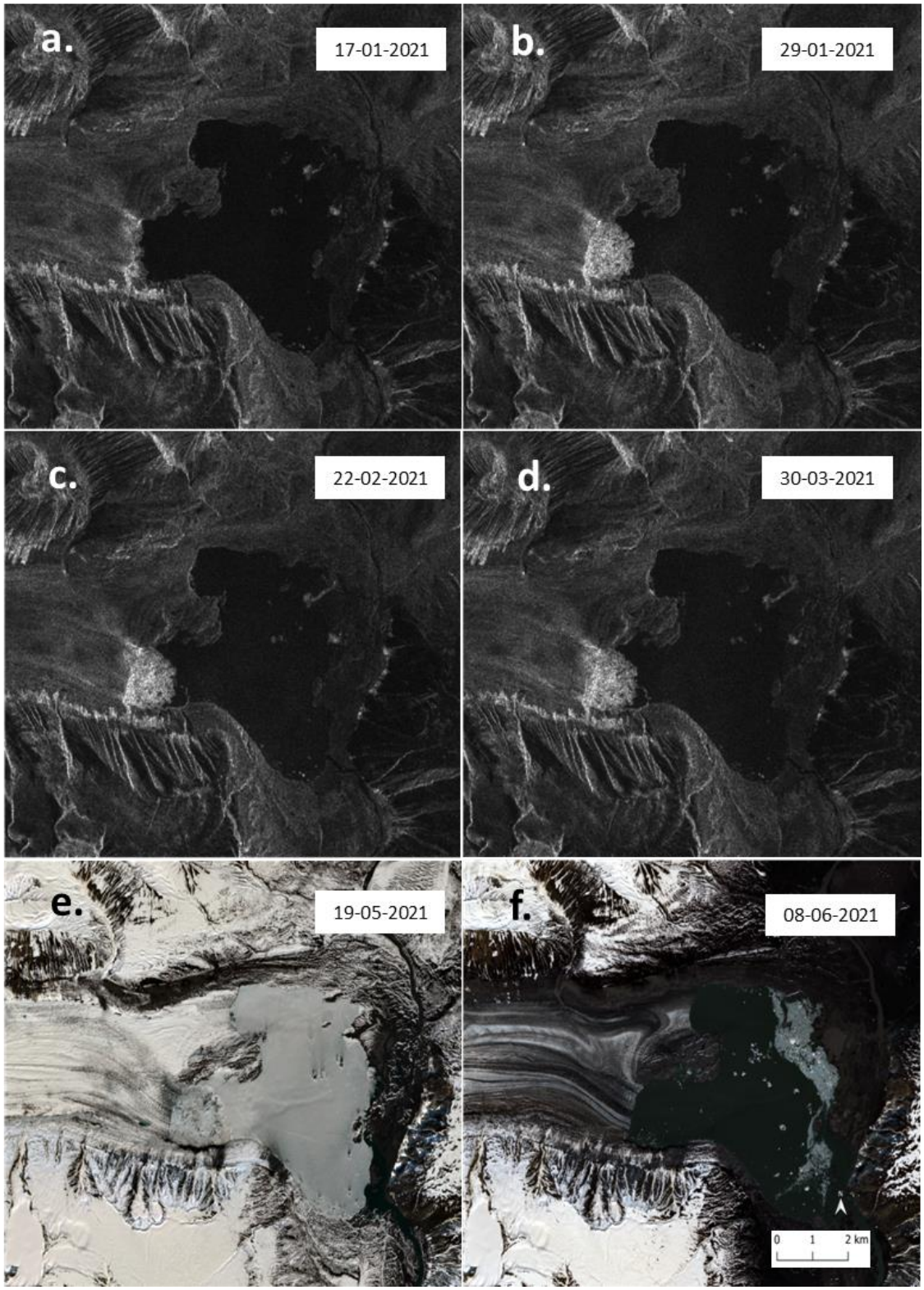

Figure A-2. Winter 2021 calving event timeline from Sentinel-1 VH imagery from (a) 2021-01-17, (b) 2021-01-29, (c) 2021-02-22, (d) 2021-03-30 and Sentinel-2 imagery from (e) 2021-05-19, and (f) 2021-06-08.

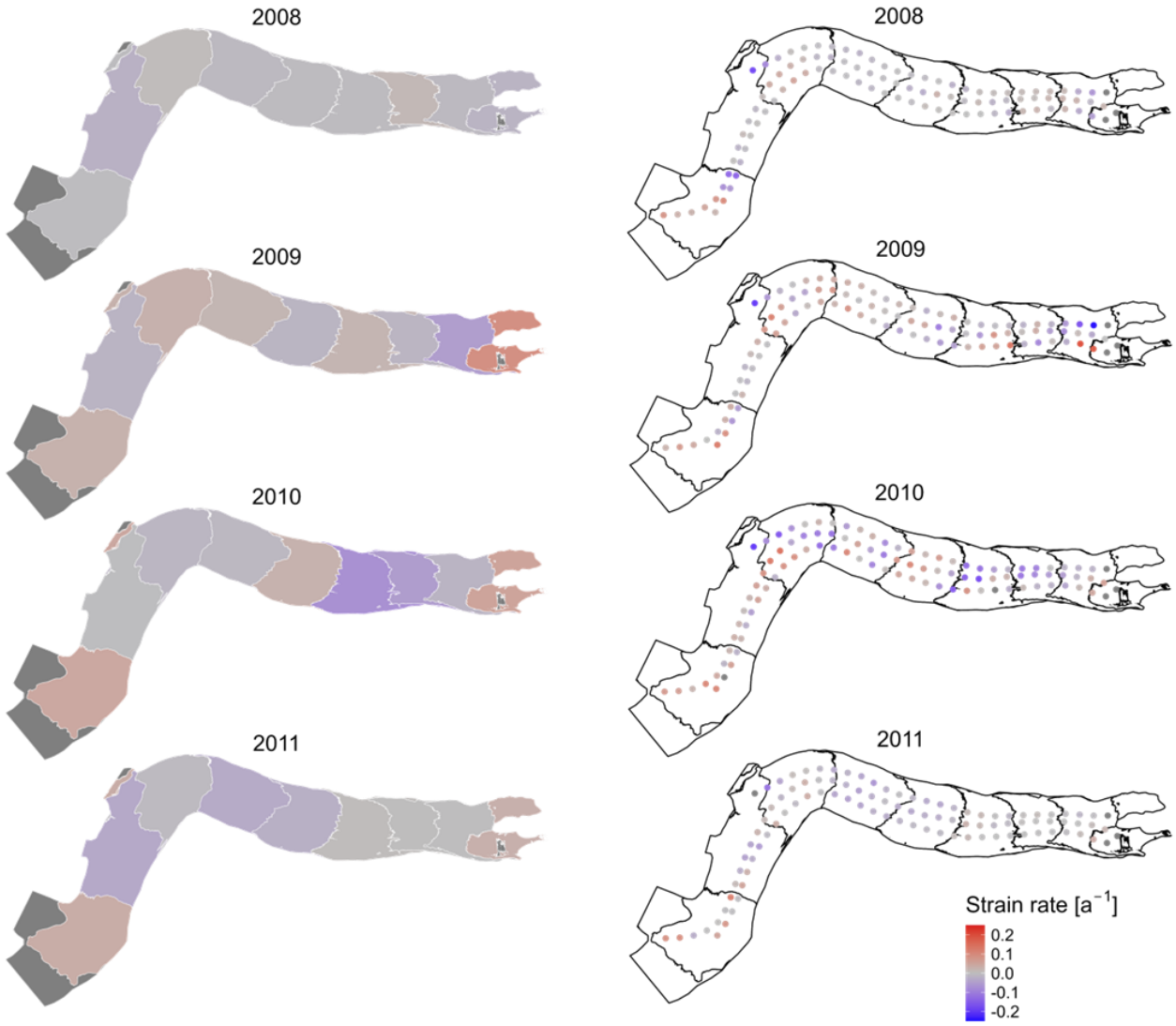

Figure A-3. Annual strain rate [a^{-1}] for each elevation band and individual points calculated from ITS_LIVE annual velocity mosaics from 2008-2011 at Nàłùdäy.

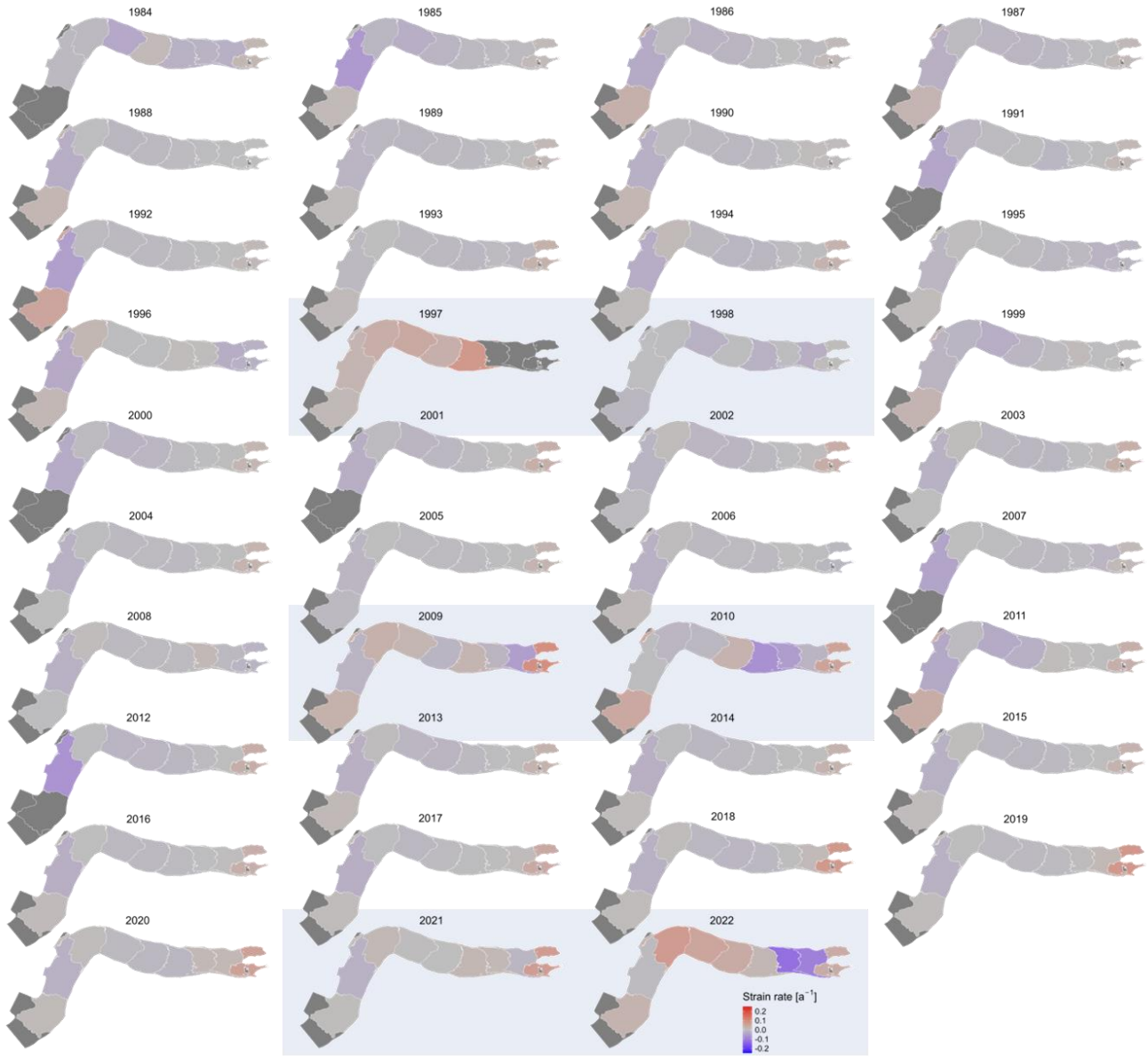

Figure A-4. Strain rate averaged and mapped by elevation band 1984-2022 derived from NASA ITS_LIVE annual velocity mosaics, with blue boxes identifying active surge phases.

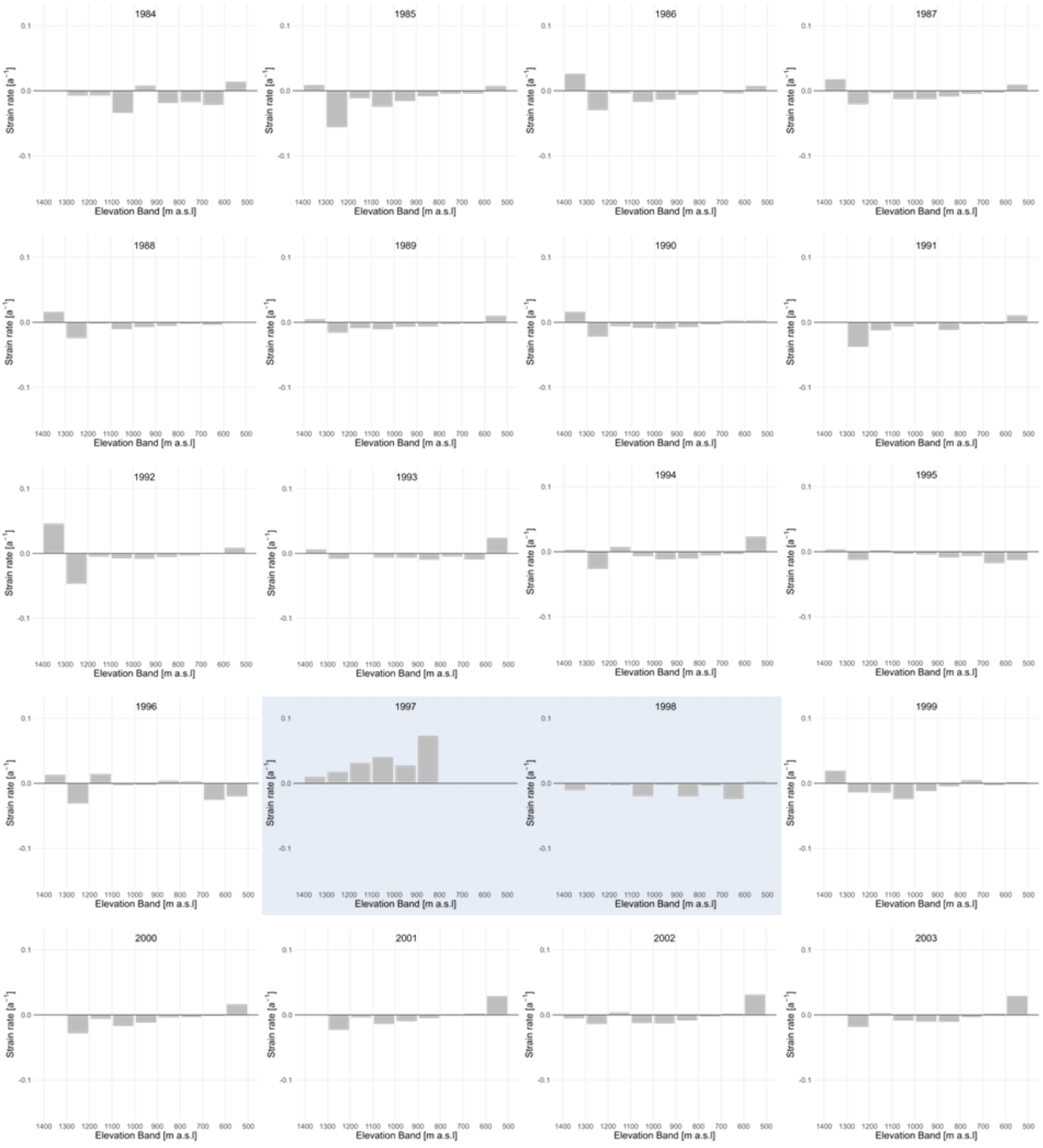
1984
1985
1986
1987
1988
1989
1990
1991
1992
1993
1994
1995
1996
1997
1998
1999
2000
2001
2002
2003
Strain rate [a⁻¹]
0.1
0.0
-0.1
1400 1300 1200 1100 1000 900 800 700 600 500
Elevation Band [m a.s.l]

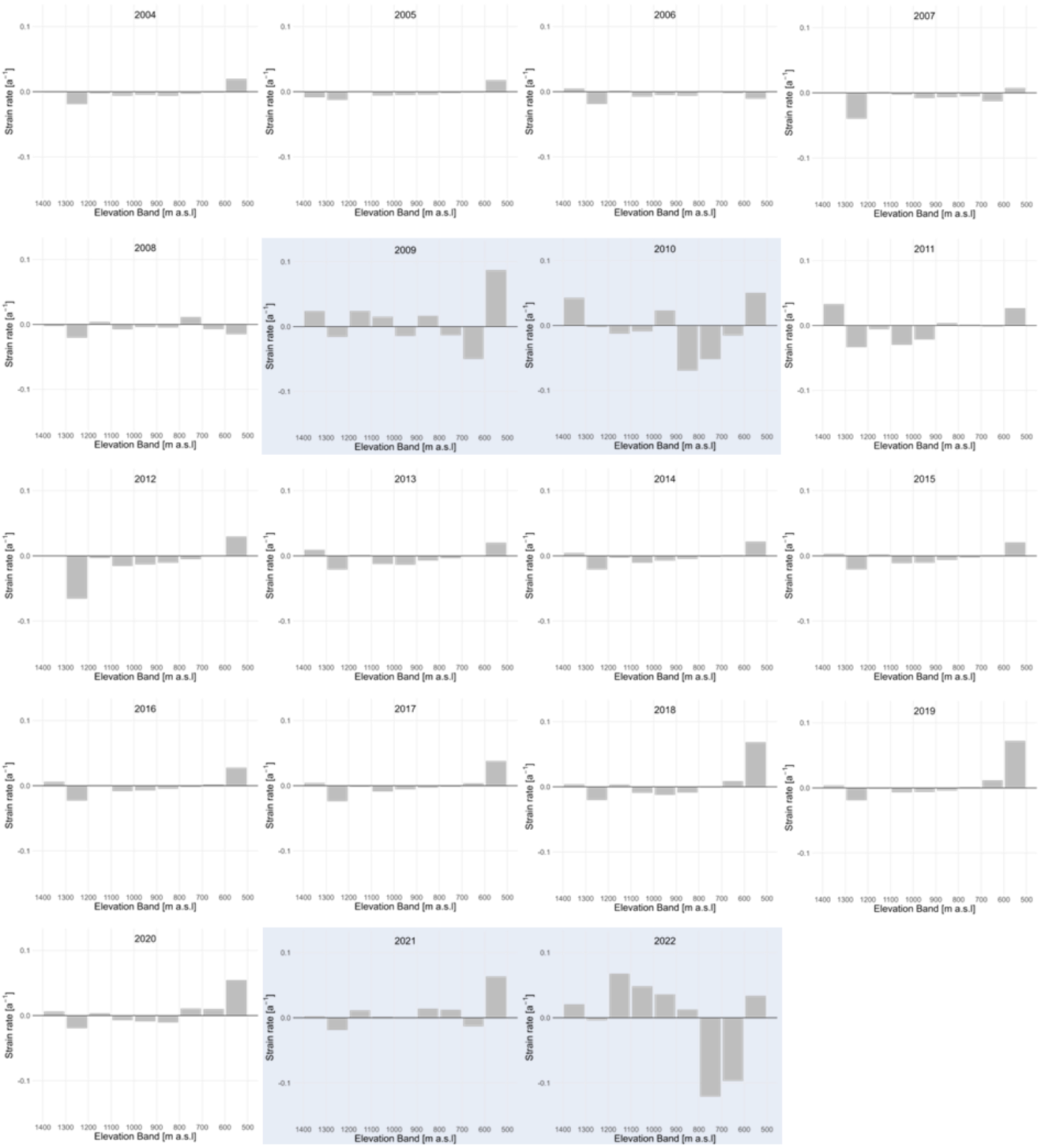

Figure A-5. Strain rate averaged by elevation band 1984-2022 derived from NASA ITS_LIVE annual velocity mosaics, with blue boxes identifying active surge phases.

Table A-2. Percent overlap between mapped streams and theoretical stream pathways in 2019 & 2023.

Stream overlap with theoretical flow pathways [%]		
Elevation band [m a.s.l.]	2019	2023
500-600	30.34	
600-700	71.82	28.30
700-800	56.53	48.82
800-900	70.09	60.31
900-1000	61.82	69.35
1000-1100	51.13	59.39
1100-1200	56.56	84.89
1200-1300	61.47	60.02
1300-1400	65.98	56.15
1400-1500	46.12	39.73
Entire Glacier	59.33	62.86